Received: 25 January 2024 | Revised: 10 June 2024 | Accepted: 13 June 2024

DOI: 10.1002/ardp.202400067

ARCH PHARM DPhG
Archiv der Pharmazie

FULL PAPER

Design, synthesis, biological evaluation, and molecular modeling simulations of new phthalazine-1,4-dione derivatives as anti-Alzheimer's agents

Demokrat Nuha[1,2,3] | Asaf Evrim Evren[1,4] | Begüm Nurpelin Sağlık Özkan[1] | Nalan Gundogdu-Karaburun[1] | Ahmet Çagri Karaburun[1]

[1]Department of Pharmaceutical Chemistry, Faculty of Pharmacy, Anadolu University, Eskişehir, Turkey

[2]Department of Chemistry, Faculty of Science, Eskisehir Technical University, Eskişehir, Turkey

[3]Faculty of Pharmacy, University for Business and Technology, Prishtina, Kosovo

[4]Vocational School of Health Services, Department of Pharmacy Services, Bilecik Seyh Edebali University, Bilecik, Turkey

Correspondence
Demokrat Nuha, Department of Pharmaceutical Chemistry, Faculty of Pharmacy, Anadolu University, 26470, Eskişehir, Turkey.
Email: demokratnuha@gmail.com and demokrat.nuha@ubt-uni.net

Funding information
None

Abstract

The development of targeted phthalazine-1,4-dione acetylcholinesterase (AChE) inhibitors for treating Alzheimer's disease involved the synthesis of 32 compounds via a multistage process. Various analytical techniques confirmed the compounds' identities. Thirteen compounds were found to inhibit AChE by more than 50% without affecting butyrylcholinesterase (BChE). Among these, three compounds, **8m**, **8n**, and **8p**, exhibited extraordinary activity similar to donepezil, a reference AChE inhibitor. During enzyme kinetic studies, compound **8n**, displaying the highest AChE inhibitory activity, underwent evaluation at three concentrations ($2 \times IC_{50}$, IC_{50}, and $IC_{50}/2$). Lineweaver–Burk plots indicated mixed inhibition activity for compound **8n** against AChE, suggesting a combination of competitive and noncompetitive characteristics. Additionally, effective derivatives **8m**, **8n**, and **8p** exhibited high blood–brain barrier (BBB) permeability in in vitro parallel artificial membrane permeability assay tests. Molecular docking studies revealed that these compounds bind to the enzyme's active site residues in a position similar to donepezil. Molecular dynamic simulations confirmed the stability of the protein–ligand system, and the chemical reactivity characteristics of the compounds were investigated using density functional theory. The compounds' wide energy gaps suggest stability and therapeutic potential. This research represents a significant step toward finding a potential cure for Alzheimer's disease. However, further research and testing are required to determine the compounds' safety and efficacy. The unique structure of phthalazine derivatives makes them suitable for various biological activities, and these compounds show promise for developing effective drugs for treating Alzheimer's disease. Overall, the development of these targeted compounds is a crucial advancement in the search for an effective treatment for Alzheimer's disease.

KEYWORDS
acetylcholinesterase inhibitor, DFT calculation, molecular docking, molecular dynamic simulation, phthalazine-1,4-dione

1 | INTRODUCTION

Alzheimer's disease (AD) is a chronic neurodegenerative condition that affects a large proportion of the world's senior population. It is the most prevalent type of dementia, characterized by progressive memory loss, cognitive decline, and behavioral changes.[1] According to the World Health Organization, 82 million people will have dementia by 2030, increasing to 152 million by 2050. AD is a complex disorder that affects numerous areas of the brain. The disease typically begins in the hippocampus, which is responsible for memory formation and storage. As the disease progresses, it spreads to other parts of the brain, resulting in the loss of cognitive functions such as speech, reasoning, and decision-making.[2]

The precise reasons for AD are still unknown. However, several risk factors that increase the likelihood of developing the disease have been identified. The most significant risk factor for developing AD is aging. People over the age of 65 are the most susceptible, and the chance rises with age. However, the disease can impact younger individuals as well, with some cases documented in people in their 40s and 50s.[3] AD is also influenced by genetic factors. A tiny proportion of instances are caused by inherited genetic mutations from one or both parents. These mutations impact the creation of beta-amyloid protein, which causes plaques to develop in the brain. Individuals who receive these mutations are almost certainly going to acquire AD at some point in their lives. Diet, exercise, and social involvement have also been shown to impact the chance of developing AD.[4]

The progression of AD involves pathophysiological hallmarks such as the accumulation of beta-amyloid plaques and tau tangles, leading to neuronal damage and cognitive decline. Neuroinflammation, oxidative stress, and synaptic dysfunction further contribute to the disease's advancement. Understanding these hallmarks is crucial for developing effective treatments and interventions for AD. AD symptoms differ from person to person, but they usually follow a predictable pattern. The most common early signs are mild memory loss and trouble with language and conversation. These symptoms worsen as the illness advances, and individuals may have trouble with everyday tasks such as dressing, bathing, and eating. In the later phases of the illness, behavioral changes such as restlessness, hostility, and hallucinations may appear.[5]

Since the beginning of the twenty-first century, numerous medications have been clinically evaluated, and numerous treatments have been proposed, including memory enhancement, inhibiting the accumulation of Ab (amyloid beta) plaques, gene therapy, neuronal function repair, and strengthening the immune response with vaccines. Despite intensive efforts, only five medications have been approved for therapeutic use.[3] Tacrine, galantamine, rivastigmine, and donepezil are cholinesterase inhibitors that have been approved for use in the therapy of AD. Memantine is an N-methyl-D-aspartate (NMDA) receptor blocker. It is used to reduce the risk of excitotoxicity caused by NMDA overstimulation. Memantine can be given alone or in combination with cholinesterase inhibitors as needed, particularly in extreme cases. It could help with the treatment of mental issues. Aducanumab and lecanumab are Food and Drug Administration (FDA)-approved monoclonal antibodies for AD. Aducanumab targets amyloid-beta plaques, potentially slowing cognitive decline, but its approval sparked controversy due to mixed trial results. Lecanumab also targets amyloid-beta, promoting plaque removal and reducing inflammation. However, it is still in clinical trials. These antibodies address the underlying pathology of Alzheimer's, offering hope for disease progression, but their exact roles, effectiveness, and safety are still debated and require more research.[5]

The cholinesterase hypothesis suggests that the reduction of cholinergic activity in the brain is a key factor in AD. Cholinesterase inhibitors, such as donepezil, are used to enhance cholinergic function and improve cognitive symptoms in Alzheimer's patients. These drugs work by preventing the breakdown of acetylcholine, a neurotransmitter, in the brain, thereby enhancing communication between nerve cells and temporarily mitigating cognitive decline.[6]

The synthesis of phthalazine derivatives involves the utilization of phthalhydrazide, a fused heterobicyclic compound with NH-acidic protons, in a three-component condensation reaction with isocyanides.[7,8] Phthalazine derivatives show numerous biological activities such as anticancer,[9,10] anti-Alzheimer,[11] antihypertensive,[12] anticonvulsant,[13] antidiabetic,[14] antimicrobial,[15] anti-inflammatory,[16] analgesic,[17] vasorelaxant,[18] and antipsychotic activities.[19] Moreover, established drugs such as burdralazine, hydralazine, ponalrestat, zopolrestat, and azelastine are obtained from corresponding phthalazinone derivatives. The generation of molecular diversity using combinatorial chemistry, particularly through solid-phase syntheses, has been a focus in organic chemistry research, offering vast libraries of structurally diverse compounds with potential therapeutic applications.[20,21]

Numerous studies have indicated that 1,4-phthalazinedione derivatives have the potential to be viable drug options for the treatment of AD. These compounds have a distinct structure that enables them to interact with the beta-amyloid protein and prevent its aggregation, which is a crucial component in AD pathogenesis. Beta-amyloid aggregation inhibition can prevent the formation of toxic oligomers and fibrils, which are thought to contribute to neuronal dysfunction and cell mortality in AD.[22] In one study, researchers examined several 1,4-phthalazinedione derivatives and discovered that some of them exhibited strong inhibitory activity against acetylcholinesterase (AChE), an enzyme involved in the breakdown of acetylcholine, a neurotransmitter essential for brain function. AChE inhibition can increase acetylcholine levels and reduce the cognitive decline associated with AD.[23]

Another study investigated the anti-inflammatory properties of 1,4-phthalazinedione derivatives and discovered that these compounds can inhibit the production of proinflammatory cytokines like interleukin-1 beta (IL-1) and tumor necrosis factor-alpha (TNF-alpha) in microglial cells, which are brain immune cells that play a role in neuroinflammation. Chronic neuroinflammation is a hallmark of AD and is thought to contribute to disease development. Furthermore, some 1,4-phthalazinedione derivatives have been found to possess strong antioxidant activity, which may help in reducing oxidative stress and inflammation associated with the illness. Oxidative stress

and inflammation can harm neurons and contribute to cognitive decline in AD.[24]

Several studies have also examined the permeability of the blood–brain barrier (BBB) to 1,4-phthalazinedione derivatives and discovered that these compounds have excellent brain penetration, which is important for drugs that target the central nervous system. Overall, the literature indicates that 1,4-phthalazinedione derivatives may be effective and safe drug options for AD therapy. Further research is needed to enhance these compounds' pharmacokinetic and pharmacodynamic characteristics, as well as to assess their safety and effectiveness in clinical studies.[25]

Based on this knowledge, we set out to develop a novel class of biologically active compounds containing this important pharmacophore. This article describes the synthesis, characterization, molecular docking studies, molecular dynamics modeling studies, density functional theory (DFT) computations, and in vitro AChE inhibitory activity of new phthalazine-1,4-dione derivatives.

2 | RESULTS AND DISCUSSION

2.1 | Chemistry

The tested compounds were synthesized via a multistep process outlined in Scheme 1. Initially, acetophenone derivatives underwent bromination to yield **2** (2-bromoacetophenone derivatives). Subsequently, methylhydrazine reacted with phthalic anhydride to produce compound **4**. Following this, sodium hydride and 2-bromoacetophenone derivatives were combined to form derivative compounds **5**. Compound **6** was synthesized by reacting ethyl 2-bromoacetate with compound **4**. Finally, various derivatives were obtained by reacting compound **7** with aldehydes. Thin-layer chromatography (TLC) and column chromatography (CMS) were employed to monitor each step, ensuring reaction completion and product purity. Recrystallization of the intended products from ethanol was performed. Melting point studies, proton nuclear magnetic resonance (^{1}H NMR) spectroscopy, carbon nuclear magnetic resonance (^{13}C NMR), high-resolution mass spectrometry (HRMS), and liquid chromatography-mass spectrometry (LCMS) were used to determine purity and structure. Supporting Information S1: Figures S8–S106 illustrate the findings.

The methylene group bound to the phenyl ring, in general, was observed as a singlet peak in a range of chemical shifts of 2.34–2.41 ppm (Ph–CH_3). The sulfonyl group displaced the methylene group linked to sulfonyl in compound **5m** to the downfield, resulting in a chemical shift of 3.32 ppm (S–CH_3). Aromatic methoxy groups in general were found as a singlet peak with chemical shifts of 3.78–3.87 ppm (Ph–OCH_3). The methylene group bound to the nitrogen atom of the 1,4-phthalazinedione ring (N–CH_3), in general, was observed as a singlet peak in a range of chemical shifts of 3.46–3.57 ppm. The methylene group bound to the nitrogen atom of the 1,4-phthalazinedione ring (N–CH_2), in general, was observed as a singlet peak in a range of chemical shifts of 4.88–5.93 ppm. The hydrogen of the imine group, in general, was found as a singlet peak with chemical shifts of 7.69–8.69 ppm (N=CH). N–N–H hydrogen was found as a broad singlet peak with chemical shifts of 11.33–11.96 ppm. The appearance of a pair of singlets, doublets, triplets, and/or multiplets with chemical shifts of 6.56–8.79 ppm was due to the aromatic protons of the aromatic rings (Ar–H).

The methylene group bound to the phenyl ring has signals between 21.41 and 21.73 ppm (Ph–CH_3). The sulfonyl group displaced the methyl group linked to sulfonyl in compound **5m** to the downfield signaled in 43.58 ppm (S–CH_3). Aromatic methoxy groups have signals that appear between 55.77 and 56.11 ppm (Ph–OCH_3). The methylene group bound to the nitrogen atom of the 1,4-phthalazinedione ring (N–CH_3) has a signal appeared between 38.80 and 38.88 ppm for **5a–5m** compounds and 63.56–64.01 ppm for **8a–8s** compounds. The methylene group bound to the nitrogen atom of the 1,4-phthalazinedione ring (N–CH_2) has a signal appeared between 68.67 and 69.30 ppm for **5a–5m** compounds and 64.81–64.98 ppm for **8a–8s** compounds. Aromatic carbons have signals that appear between 102.52 and 194.02 ppm.

The mass analysis includes determining the mass/charge (*m/z*) ratios of each compound. Theoretical values were determined and compared with the observed results. Each study produced a number with greater than 90% accuracy with an error margin of 0.05. This indicates that the names of the compounds have been verified and match with the NMR data. The spectra show that each molecule has a primary peak $[M+1]^+$ that is linked to its molecular weight. All spectra and analytical data for the compounds were included in the analytical papers of Supporting Information S1: Figures S8-S103.

2.2 | Absorption, distribution, metabolism, and excretion (ADME) parameters

An in silico ADME analysis of compounds **5a–5m** and **8a–8s** was conducted using the SwissADME web tool, and important physicochemical parameters were identified.[26,27] The values of rotatable bonds (RB), the number of hydrogen bond acceptors (HBA), the number of hydrogen bond donors (HBD), the topological polar surface area (TPSA), lipophilicity (Log P), solubility (Log S), skin permeation (Log K), gastrointestinal absorption (GIA), and other parameters are presented in Supporting Information S1: Table S1.

The single most important physical characteristic affecting a drug's efficacy, distribution, and elimination in the body is lipophilicity (fat-likeness). Lipophilicity is the most commonly used metric in drug discovery and SAR studies because no other physical feature has been demonstrated to influence as many biological factors as lipophilicity. The results of the lipophilicity indicator LogP(o/w) computation fell within the range reported by Daina et al.,[28] which is between −0.7 and 5. The lipophilicity of the selected substances (**5a–5m** and **8a–8s**) ranged from 1.1 to 3.58. In general, **5a–5m** compounds had higher lipophilicity values than **8a–8s** compounds. This could explain why **8a–8s** molecules have minimal BBB

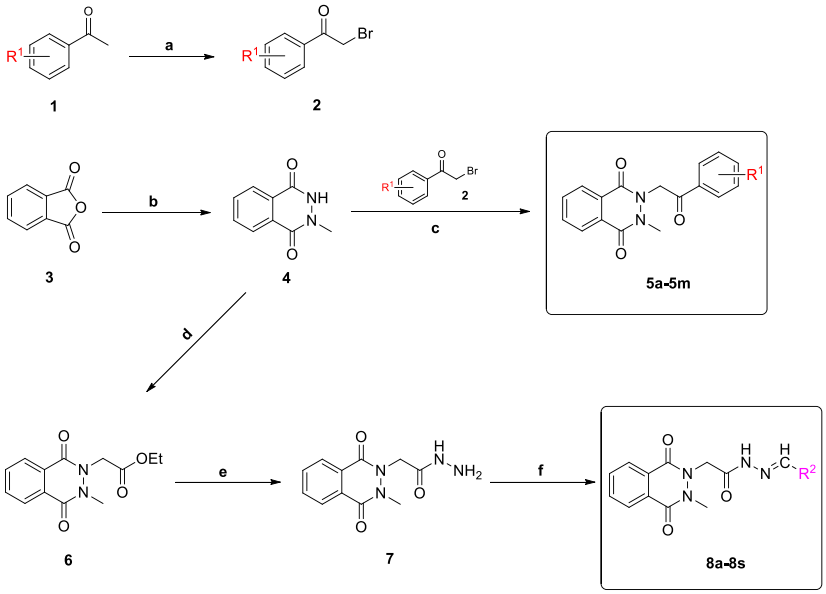

SCHEME 1 The synthesis diagram of the compounds **5a–5m** and **8a–8s**. Reagents and conditions: (a) CH_3COOH, HBr, Br_2, 80°C, 2–8 h; (b) CH_3COOH, CH_3NHNH_2, 125°C, 5 h; (c) dimethylformamide (DMF), NaH, room temperature, 2 d; (d) DMF, ethyl 2-bromoacetate, K_2CO_3, room temperature, 2 h; (e) EtOH, $N_2H_4 \times H_2O$, room temperature, 12 h; and (f) EtOH, aldehyde derivatives, 80°C, 3–5 h.

Compound code	R^1	R^2
5a	-F, *p*	/
5b	-Cl, *p*	/
5c	-H, *p*	/
5d	-CH_3, *p*	/
5e	-OCH_3, *p*	/
5f	-NO_2, *p*	/
5g	-CN, *p*	/
5h	-Cl, *m*	/
5i	-NO_2, *m*	/
5j	-3,4-di Cl	/
5k	-naphthalen-2-yl	/
5l	-([1,1'-biphenyl]-4-yl)	/
5m	-methyl-sulfonyl, p	/
8a	/	Phenyl
8b	/	4-Bromophenyl
8c	/	4-Fluorophenyl
8d	/	4-Chlorophenyl
8e	/	4-Methylphenyl
8f	/	4-Methoxyphenyl
8g	/	3,5-Dimethoxyphenyl
8h	/	3,4-Dihydroxyphenyl
8i	/	Naphthalene-1-yl
8j	/	Naphthalene-2-yl
8k	/	6-Methoxy-naphthalene-2-yl
8l	/	Thiophen-2-yl
8m	/	Furan-2-yl
8n	/	1*H*-Pyrrol-2-yl
8o	/	5-Bromo-2-hydroxyphenyl
8p	/	2-Nitrophenyl
8q	/	3-Nitrophenyl
8r	/	2,6-Dichlorophenyl
8s	/	3,4-Dichlorophenyl

permeability. The water solubility numbers (Log S) calculated came within the required range, which is between (−6.5) and (5). The water solubility values of the designated substances (**5a–5m** and **8a–8s**) ranged from (−4.83) to (−2.62) and were all higher than those of the standard drug.

When absorbance and permeability in different bodily parts were assessed, it was predicted that the absorption of the targeted drugs from the gastrointestinal tract (GIA) would be very similar to that of the reference drug. The prediction model correlates the compounds' polarity and lipophilicity and elucidates their relationship to BBB permeability.[28] Because all the drugs created for this study were intended to target AChE in the central nervous system, BBB permeability should be high or increased central nervous system (CNS). Loading molecules **8a–8s** onto a drug transport substrate permeable through the BBB is one way to enhance their bioavailability in the CNS. Nanotechnology has been employed to develop such medication delivery techniques, effectively addressing several bioavailability issues.[29] Aside from lipophilicity, the **8a–8s** substances had TPSA that were high enough to indicate inadequate BBB permeability.

2.3 | In vitro AChE and butyrylcholinesterase (BChE) inhibition tests

The designated compounds **5a–5m** and **8a–8s** were evaluated for their ability to inhibit both AChE and BChE. The tests involved colorimetric measurements of the ligand–enzyme complexes formed by incubating both components in vitro. The test protocol, as well as the underlying analytical approach, are explained by Saglk.[30] The testing and analysis took place in two phases. In the first phase, the proportion of inhibition was calculated for each molecule evaluated at both 10^{-3} and 10^{-4} M concentrations. Table 1 summarizes the results, including the inhibition percentage and standard deviation (SD). In the second phase, lower doses down to 10^{-9} M were evaluated for compounds that demonstrated more than 50% inhibitory activity at the measured concentrations. Table 1 summarizes the results. Donepezil and tacrine were chosen as standard reference compounds for AChE and BChE inhibition.

The results from the first stage revealed that 13 compounds had more than 50% inhibition against AChE: **5a**, **5b**, **5e**, **5f**, **5i**, **8c**, **8d**, **8f**, **8h**, **8m**, **8n**, **8p**, and **8q**, with inhibition percentages ranging from 81% to 94%. However, no activity within the specified limit of 50% was observed for BChE inhibition. Consequently, no further BChE tests were conducted.

Based on the findings of AChE activity, it was found that different substituents attached to the benzene ring significantly impacted the biological activity of compounds **5a–5m**. Table 1 indicates that the molecule without a benzene ring substituent (**5c**) exhibited modest activity at 10^{-4} M, with 41% inhibition. When inductive electron-withdrawing substituents were attached to the benzene rings, their biological activity increased. This was observed in compounds **5a**, **5b**, and **5e**, where –F, –Cl, and –OCH3 were connected in the para position, resulting in very good activity, with 81% inhibition at 10^{-4} M. Conversely, when mesomeric electron-withdrawing substituents were attached to the benzene rings, their biological activity further increased. This was seen in molecules **5f** and **5i**, which had $-NO_2$ substituents in the *para* and *meta* positions, with 85% and 87% inhibition at 10^{-4} M, respectively. In contrast, when substituents with inductive electron-donating properties were attached to the benzene rings, their biological activity decreased, as in the case of **5d**, which exhibited 45% inhibition at 10^{-4} M and had a $-CH_3$ substituent.

Similarly, various substituents attached to the benzene ring had a significant effect on the biological activity of compounds **8a–8s**, as indicated by AChE activity data. Table 1 shows that the molecule **8a**, lacking a benzene ring ligand, had low activity with 42% inhibition at 10^{-4} M. The biological activity of inductive electron-withdrawing substituents increased when they were attached to the benzene rings. This was observed in **8c**, **8d**, and **8f**, which contained –F, –Cl, and $-OCH_3$ in the para position and demonstrated strong activity at 10^{-4} M, with 91%, 86%, and 81% inhibition, respectively. The biological activity further increased when substituents were attached to mesomeric electron-withdrawing benzene rings. This was seen in molecules **8p** and **8q**, which had $-NO_2$ substituents in the ortho and meta positions and exhibited 92% and 91% inhibition, respectively, at 10^{-4} M. On the other hand, when inductive electron-donating substituents were incorporated into the benzene rings, their biological activity decreased, as observed in **8e**, which had 37% inhibition at 10^{-4} M and included a $-CH_3$ substituent. Notably, when a five-membered heterocyclic ring was connected to the core molecule instead of the benzene ring, as in **8m** and **8n**, where furan and pyrrole were attached instead of benzene, a substantial increase in biological activity was observed at 10^{-4} M, with 90% and 94% inhibition, respectively.

Table 2 outlines the inhibition percentages and IC_{50} values, which represent the concentration of a compound required to inhibit 50% of the enzymatic activity for the most potent inhibitors of AChE alongside the well-known reference compound donepezil. Additionally, the IC_{50} values offer quantitative insight into the concentration-dependent inhibitory effects, aiding in the determination of the most effective compounds. By providing this comprehensive data, Table 2 facilitates the evaluation and prioritization of potential candidates for further development as therapeutic agents targeting conditions such as AD.

From all of the targeted compounds, three have shown exquisite activities: **8m**, **8n**, and **8p**. **8m** showed 90.196% ± 2.648% inhibition in 10^{-4} M and their IC_{50} values were 0.039 μM ± 0.001 μM. **8n** showed 94.368% ± 3.029% inhibition in 10^{-4} M and their IC_{50} values were 0.033 μM ± 0.001 μM. **8p** showed 92.379% ± 2.136% inhibition in 10^{-4} M and their IC_{50} values were 0.036 μM ± 0.001 μM.

The similarities in the main sections of the compounds with donepezil, as shown in Figure 1, explain why these compounds have such strong inhibitory activity against AChE. To begin, these are phthalazine-1,4-dione compounds. Second, by forming hydrophobic contacts and pi–pi stacking with the enzyme's neighboring amino acid residues, the phthalazine-1,4-dione ring can mimic the indanone of

TABLE 1 % Inhibition of targeted compounds, donepezil, and tacrine against AChE and BChE, along with IC_{50} values.

Compounds	AChE % inhibition		AChE IC_{50} (μM)	BChE % inhibition		BChE IC_{50} (μM)
	10^{-3} M	10^{-4} M		10^{-3} M	10^{-4} M	
5a	92.196±2.719	81.257±1.420	0.108±0.005	52.727±0.962	36.523±0.853	>100
5b	88.028±2.026	81.174±1.862	0.237±0.010	50.561±1.157	44.951±0.908	>100
5c	63.527±2.351	41.569±1.548	>100	28.984±0.822	20.627±0.861	>1000
5d	69.962±2.036	45.345±1.010	>100	35.127±0.796	23.764±0.876	>1000
5e	90.720±1.356	81.621±1.781	0.155±0.006	31.089±0.963	28.185±0.728	>1000
5f	91.411±2.562	85.820±1.796	0.067±0.003	55.337±1.241	30.891±0.836	>100
5g	69.956±1.919	40.647±1.873	>100	33.581±1.074	24.364±0.991	>1000
5h	74.318±2.682	44.519±0.905	>100	30.149±0.822	20.677±0.835	>1000
5i	92.529±1.809	87.602±1.354	0.059±0.002	57.667±1.384	42.160±1.255	>100
5j	75.841±2.861	42.651±0.837	>100	28.420±0.884	21.728±0.826	>1000
5k	48.662±1.923	37.384±0.946	>1000	36.848±1.051	33.661±0.937	>1000
5l	45.803±1.147	35.467±0.727	>1000	31.303±0.807	27.507±1.037	>1000
5m	77.157±2.961	46.629±1.659	>100	37.626±1.132	25.759±0.847	>1000
8a	68.496±2.548	42.050±0.974	>100	35.998±1.320	30.437±0.867	>1000
8b	74.655±3.242	45.162±0.862	>100	30.110±0.967	22.362±0.858	>1000
8c	95.207±2.829	91.618±2.065	0.044±0.002	28.448±0.916	26.904±0.720	>1000
8d	89.921±1.997	86.306±2.262	0.212±0.009	38.567±1.458	32.297±1.562	>1000
8e	65.312±1.851	37.621±0.833	>100	41.761±1.499	36.837±0.930	>1000
8f	92.162±2.217	82.681±2.035	0.091±0.004	61.820±1.899	41.081±1.204	>100
8g	73.586±3.038	40.957±0.941	>100	30.227±0.976	21.664±0.863	>1000
8h	93.244±3.120	89.368±2.679	0.055±0.002	35.619±1.361	26.795±0.985	>1000
8i	41.652±0.922	32.168±0.865	>1000	39.338±1.736	32.637±1.055	>1000
8j	43.364±1.384	36.757±0.931	>1000	31.855±1.312	28.281±0.990	>1000
8k	45.418±1.427	38.994±1.067	>1000	36.918±1.534	27.497±0.822	>1000
8l	78.611±2.466	43.712±1.261	>100	30.167±0.862	24.051±0.739	>1000
8m	97.268±3.258	90.196±2.648	0.039±0.001	60.510±2.021	42.665±0.962	>100
8n	98.124±2.716	94.368±3.029	0.033±0.001	65.724±2.174	36.784±0.753	>100
8o	64.728±2.071	32.216±0.905	>100	26.689±0.891	21.537±0.857	>1000
8p	97.549±2.794	92.379±2.136	0.036±0.001	64.467±1.903	40.291±1.336	>100
8q	94.428±2.658	91.612±2.036	0.049±0.002	34.248±1.066	31.123±0.864	>1000
8r	77.418±2.861	48.108±1.849	>100	38.851±1.652	33.961±0.918	>1000
8s	69.296±2.158	39.357±1.131	>100	42.636±1.985	35.474±0.832	>1000
Donepezil	99.156±1.302	97.395±1.255	0.0201±0.0014	-	-	-
Tacrine	-	-	-	99.827±1.378	98.651±1.402	0.0064±0.0002

Abbreviations: AChE, acetylcholinesterase; BChE, butyrylcholinesterase.

donepezil in 268. Third, the carbonyl group found in indanone was moved to the outside in the benzofuran derivatives, but it was expected to act as a HBA just like the carbonyl of indanone. Fourth, the hydrazide in the central structure is the piperidine equivalent of donepezil. Fifth, the counterpart of the benzyl group in the core structure of the most active molecules, which forms a hydrophobic link with specific residues in the enzyme's active site pocket, is the furan, pyrrole, and benzene ring. (**8m**, **8n**, and **8p**, respectively).

TABLE 2 Inhibition% and IC_{50} values of the most potent inhibitors and donepezil for AChE.

Compound	AChE inhibition %							IC_{50} (μM)
	10^{-3} M	10^{-4} M	10^{-5} M	10^{-6} M	10^{-7} M	10^{-8} M	10^{-9} M	
5a	92.196±2.719	81.257±1.420	76.059±2.015	72.036±1.874	48.915±0.997	18.468±0.712	15.715±0.739	0.108±0.005
5b	88.028±2.026	81.174±1.862	70.548±2.110	68.306±2.055	41.062±1.734	30.401±1.095	18.468±0.741	0.237±0.010
5e	90.720±1.356	81.621±1.781	72.026±1.741	70.801±2.058	46.187±1.895	26.6481.104	20.117±0.955	0.155±0.006
5f	91.411±2.562	85.820±1.796	78.206±2.147	70.856±1.420	58.458±1.184	41.056±1.024	20.459±0.836	0.067±0.003
5i	92.529±1.809	87.602±1.354	82.569±2.421	78.914±2.057	60.819±1.997	45.802±1.304	22.230±1.055	0.059±0.002
8c	95.207±2.829	91.618±2.065	84.511±1.941	74.692±2.185	67.201±1.719	44.71±0.937	25.529±0.884	0.044±0.002
8d	89.921±1.997	86.306±2.262	72.102±2.336	69.679±1.352	45.759±1.264	29.313±0.919	22.759±0.820	0.212±0.009
8f	92.162±2.217	82.681±2.035	74.588±2.084	67.136±1.920	55.414±1.557	37.569±1.236	20.748±0.987	0.091±0.004
8h	93.244±3.120	89.368±2.679	86.123±1.932	70.518±1.574	63.268±2.169	44.057±1.948	22.116±1.051	0.055±0.002
8m	97.268±3.258	90.196±2.648	85.424±2.685	74.058±2.151	64.727±1.969	46.948±1.774	20.627±1.036	0.039±0.001
8n	98.124±2.716	94.368±3.029	82.095±2.621	74.411±2.069	67.364±1.984	45.75±1.251	21.548±0.933	0.033±0.001
8p	97.549±2.794	92.379±2.136	87.136±1.952	78.512±2.439	68.579±1.551	44.029±1.821	21.967±0.945	0.036±0.001
8q	94.428±2.658	91.612±2.036	83.124±2.336	72.996±2.097	64.402±1.785	41.957±1.251	21.128±0.923	0.049±0.002
Donepezil	99.156±1.302	97.395±1.255	93.583±1.167	91.277±1.074	76.982±0.951	35.459±0.453	18.410±0.411	0.021±0.0009

Abbreviation: AChE, acetylcholinesterase.

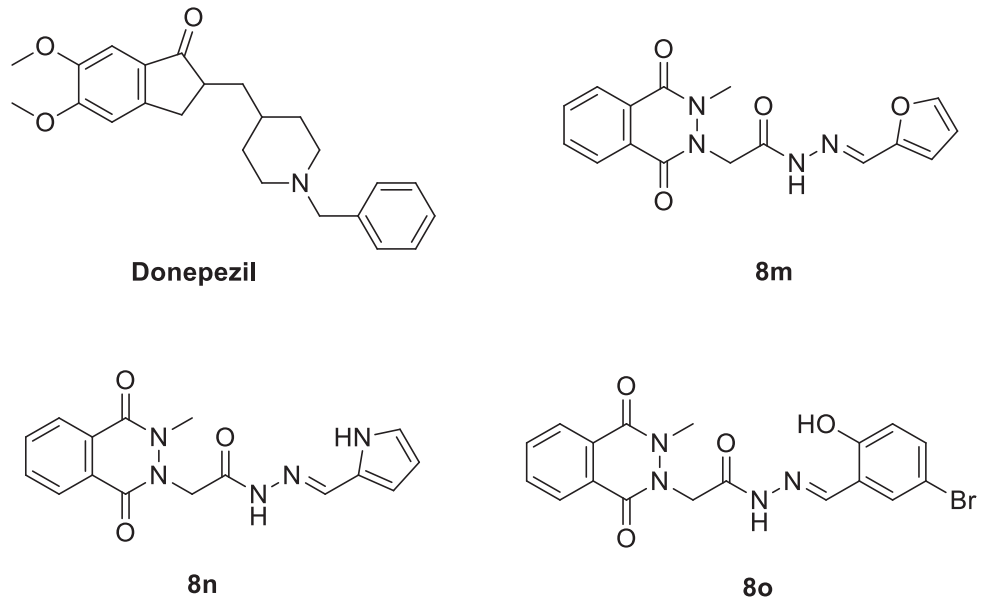

FIGURE 1 The chemical structures of the most active compounds in comparison to donepezil.

2.4 | Evaluation of enzyme kinetic studies

For the kinetic studies, the compound **8n**, which was found to have the highest inhibitory activity on the AChE enzyme, was selected. Unlike enzyme activity experiments, inhibitor compounds were prepared at three different concentrations, $2 \times IC_{50}$, IC_{50}, and $IC_{50}/2$. The method was applied in two different ways, in the presence and absence of an inhibitor. The Lineweaver–Burk plot was drawn using the absorbance values and substrate concentrations obtained because of the tests. The graphs show 1/S (1/substrate concentrations) on the x-axis and 1/absorbance values representing 1/V on the y-axis (Figure 2). In the graphs, there are four different lines belonging to the concentrations of the test compounds at $2 \times IC_{50}$, IC_{50}, and $IC_{50}/2$ values and the control group, that is, the enzyme kinetic experiment performed in the absence of inhibitory substances. Depending on where these four lines intersect on the graph, the type of reaction between the substrate and the inhibitor against the enzyme is decided.

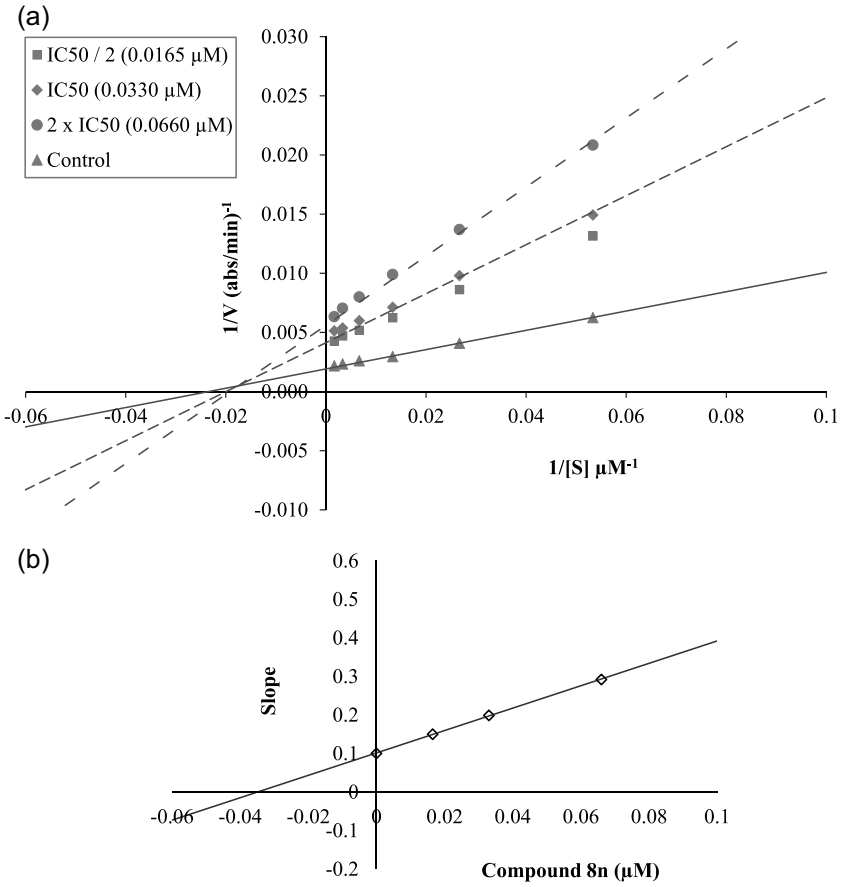

FIGURE 2 (a) Lineweaver–Burk plots for the inhibition of acetylcholinesterase (AChE) by compound **8n**. [S], substrate concentration (µM); V, reaction velocity (nmol/min/mg protein). Inhibitor concentrations are shown at the left. (b) Secondary plot (Dixon plot) for the calculation of the steady–state inhibition constant (K_i) of compound **8n**. K_i was calculated as 0.0349 µM.

Enzyme inhibition is generally divided into two categories: reversible and irreversible. In irreversible inhibition, the inhibitor either covalently binds to the enzyme or forms a poorly dissociated complex. Reversible inhibition is divided into four groups: mixed type, competitive, noncompetitive, and semi-competitive (uncompetitive) inhibition types. In Lineweaver–Burk plots, it is defined as follows: if the four lines are parallel to each other, it is uncompetitive inhibition; if they intersect on the y-axis, it is competitive inhibition; if the intersection is on the x-axis, it is noncompetitive inhibition; and if there is an intersection within the regions of the graph without being on the axes, it is mixed inhibition.[31–34]

Compound **8n**, which was the most effective derivative against the AChE enzyme, was selected for enzyme kinetic studies. The Lineweaver–Burk curves obtained as a result of the enzyme kinetic studies of compound **8n** on the AChE enzyme (Figure 2) showed that the four lines intersected in the area outside of the axes. According to the Lineweaver–Burk curves, compound **8n** had mixed inhibition activity on the AChE enzyme.

2.5 | In vitro BBB permeability assay (parallel artificial membrane permeability assay [PAMPA])

To evaluate the BBB permeability of the effective derivatives **8m**, **8n**, and **8p**, in vitro parallel artificial membrane permeability assay (PAMPA) tests were applied. The obtained results are presented in Table 3. Compounds **8m**, **8n**, and **8p** were found to have high BBB permeability.

2.6 | Molecular docking results

Molecular docking was employed to evaluate the interactions of the active compounds **8m**, **8n**, and **8p** with the AChE active site residues. Since no effect against BChE was observed, molecular docking studies for this enzyme were unnecessary. AChE inhibitors operate by binding to either the catalytic anionic site (CAS) or the peripheral anionic site (PAS) or both simultaneously, spanning the entire active site region of the enzyme. Key CAS amino acids that serve as binding sites for inhibitor medications include Serine (Ser)-203, Glutamic acid (Glu)-334, Histidine (His)-447, Tryptophan (Trp)-86, Tyrosine (Tyr)-130, Tyr-133, Tyr-337, and Phenylalanine (Phe)-338. PAS includes amino acids such as Tyr-72, Aspartic acid (Asp)-74, Tyr-124, Tyr-341, and Trp-286.[30]

When examining the docking positions of **8m**, **8n**, and **8p**, it was observed that they attached to the AChE enzyme in a manner similar to donepezil. Upon investigating the chemical structures of these related compounds, it was evident that they formed an aromatic structure comprising phthalazine-1,4-dione and benzene rings, combined with a polar structure resembling hydrazide. According to the docking positions of these compounds, the aromatic structure

TABLE 3 Type of BBB penetration of compounds 8m, 8n, and 8p.

Classification	Type of BBB permeation	Compound	Type of BBB permeation
CNS+	High BBB permeation P_e (10^{-6} cm s^{-1}) > 4.0	**8m**	CNS+ High BBB permeation
		8n	CNS+ High BBB permeation
		8p	CNS+ High BBB permeation
CNS−	Low BBB permeation P_e (10^{-6} cm s^{-1}) < 2.0		
CNS±	BBB permeation uncertain 2.0 < P_e (10^{-6} cm s^{-1}) < 4.0		

Abbreviation: BBB, blood–brain barrier; CNS, central nervous system.

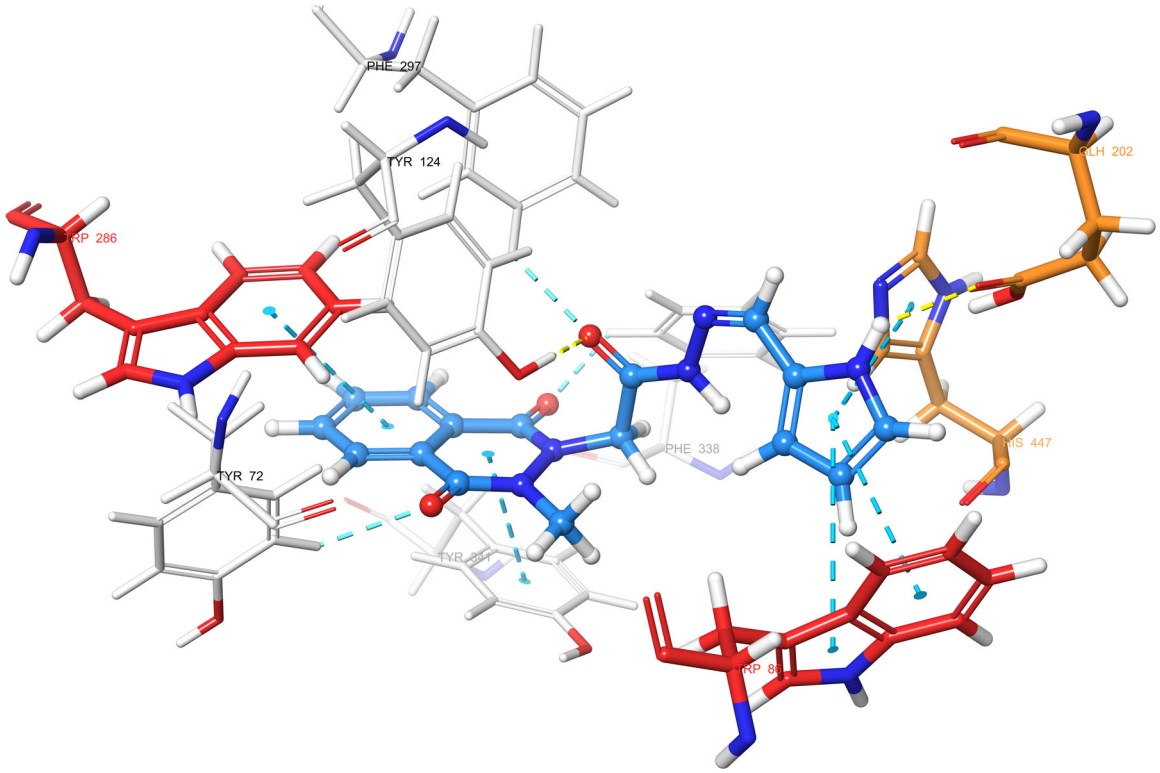

FIGURE 3 Compound **8m**'s three-dimensional pose and interactions at the acetylcholinesterase (AChE) active site.

was situated in the PAS area of the enzyme's active region, while the polar structure interacted with the CAS region. Similar to donepezil, these related chemicals interacted with the DBS (donepezil binding site) and aggregated on the enzyme's active site.

Further investigation of compound **8m's** docked pose, in terms of ligand–enzyme interactions, as depicted in Figures 3 and 4, revealed that compound **8m** established interactions between the furan ring and the key amino acids Trp-86 and His-447 in CAS and the phthalazine-1,4-dione ring with Trp-286 in PAS. These interactions mirrored those formed by donepezil. The association between the phthalazine-1,4-dione ring of compound **8m** and the phenyl ring of the Tyr-341 amino acid played a crucial role in attaching it to the enzyme's active site. Additionally, the carbonyl group in the molecule formed an H-bond with the phenyl ring of Tyr-124.

Examining compound **8n**'s docked pose in terms of ligand–enzyme interactions, as illustrated in Figures 5 and 6, revealed that compound **8n** established interactions between the pyrrole ring and the key amino acids Trp-86 and His-447 in CAS, and the phthalazine-1,4-dione ring with Trp-286 in PAS. The association between the phthalazine-1,4-dione ring of compound **8n** and the phenyl ring of the Tyr-341 amino acid played a crucial role in attaching it to the enzyme's active site. Additionally, the carbonyl group in the molecule formed an H-bond with the phenyl ring of Tyr-124. The nitrogen element in the pyrrole ring also formed an H-bond with the phenyl ring of Glu-202.

Analyzing compound **8p's** docked conformation in terms of ligand–enzyme interactions, as depicted in Figures 7 and 8, reveals that compound **8p** established interactions between the phthalazine-1,4-dione ring with Trp-286 and Tyr-341 in PAS and the benzene ring with

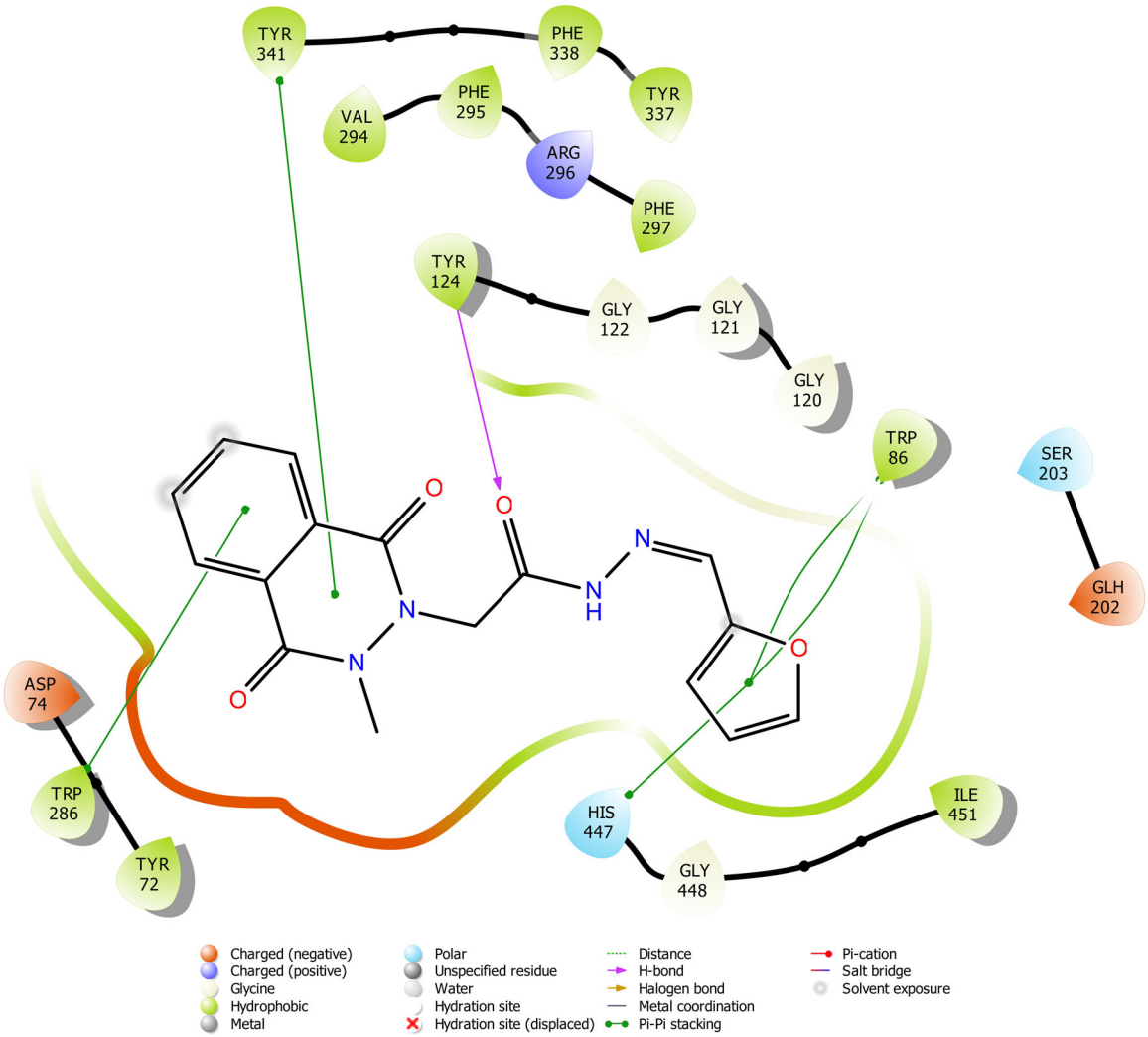

FIGURE 4 Compound **8m**'s two-dimensional pose and interactions at the acetylcholinesterase (AChE) active site.

Tyr-337 in CAS. These interactions play a crucial role in binding to the active region of the enzyme. In CAS, the Nitro group formed a pi–cation stacking interaction with the important amino acid Trp-86. Additionally, the carbonyl group in the molecule created an H-bond with the phenyl ring of Tyr-124. The oxygen atom in the nitro group also established H-bonds with the phenyl rings of Gly-121 and Glu-202.

2.7 | Molecular dynamics simulation results

Complexes gain a better understanding of the effects of environmental variations and categorize the structure–activity relationship (SAR). Figure 9 presents the results. In both cases, the system's stability was maintained (Figure 9a,b). The radius of gyration (RG) plot clearly demonstrated that when compound **8n** underwent a slight conformational change around 45 ns (as shown in Supporting Information S1: Supporting Video S1 and Figure 4.58), the other graphs the root mean square deviation (RMSD) and root mean square fluctuation (RMSF) suggested that the complex's stability remained intact. This aligns with the stability rules as originally explained.[35] The RMSF values of theloop region (depicted as a white band in the RMSF plot) that interacted with the ligand in this study remained below 0.8. Furthermore, the α-helix (red band) and β-sheets showed minimal change, with values also less than 0.8. The RMSD value for the protein fluctuated between 1 and 3. All of these findings indicate the stability of the protein–ligand system throughout the experiment. Therefore, the relationships established through molecular dynamics simulation (MDS) are reliable.

In Figure 9c,d, the H-bonds, water-mediated H-bonds, aromatic H-bonds, and stackings are illustrated. Interactions with Trp86 (stackings), Tyr124 (H-bond), Tyr341 (stackings), Tyr337 (stackings), and Phe295 (H-bond) were consistently maintained during the experiment. The ligand also showed a slight shift from Trp286 to Arg493 in the PAS region. Although the acetamide moiety is located in the active site, similar to the enzyme-substrate (acetylcholine), it does not bind with Ser203 or Trp286 residues. Instead, it likely forms interactions with Tyr124 and Phe295 residues, leading to their relocation to the PAS region (see Figure 8 and the accompanying video). As previously mentioned, Arg493 reaches the active-site

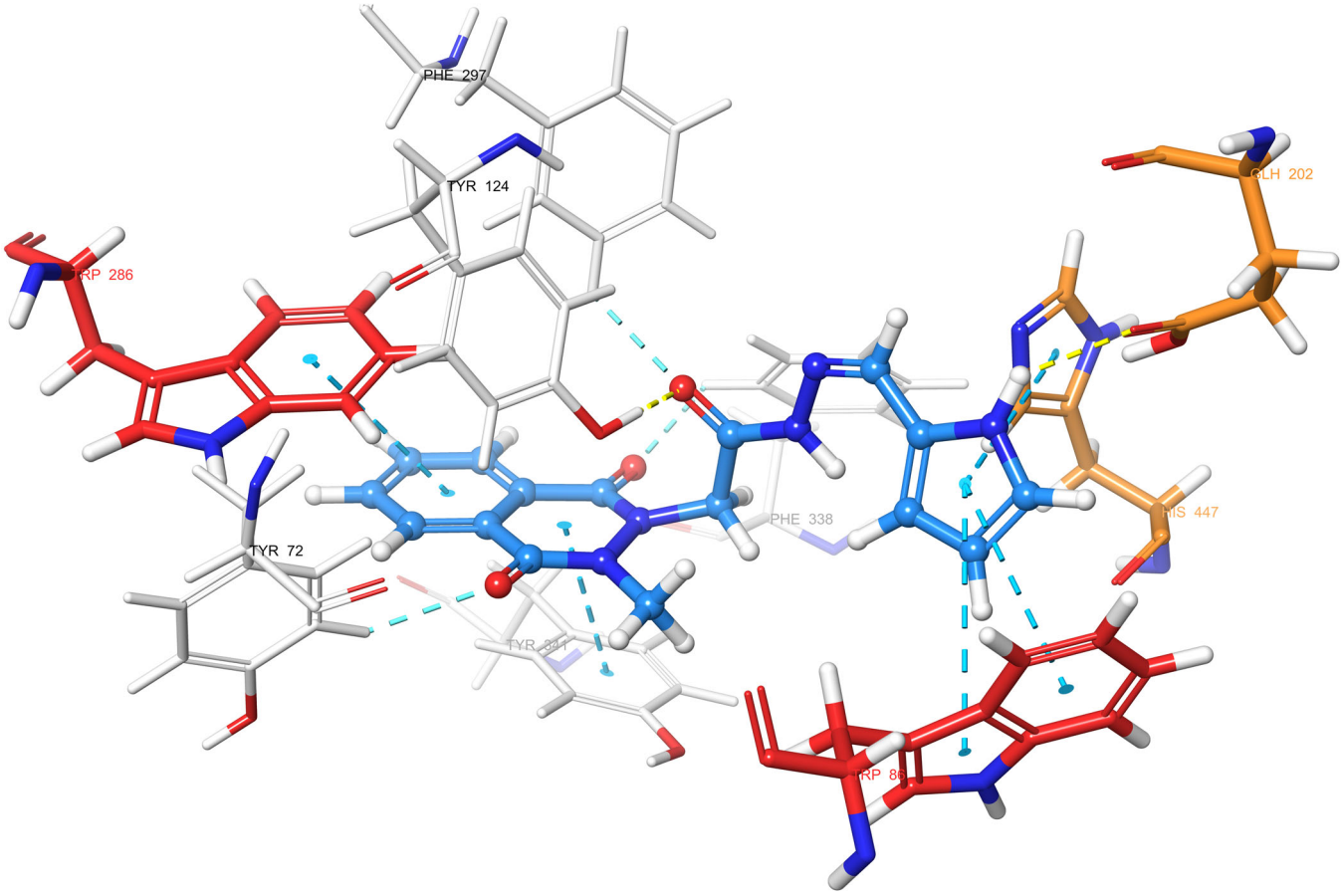

FIGURE 5 Compound **8n**'s three-dimensional pose and interactions at the acetylcholinesterase (AChE) active site.

gorge and forms a stacking interaction with Trp286 (a PAS amino acid). Consequently, this and other PAS residues (such as Tyr124) that may interact with this loop contribute to the increased inhibitory activity. In this study, compound **8n** formed direct H-bonds with Tyr124 through its two different moieties, the acetamide linker and the pyrrole ring. While no direct interaction with Trp286 was observed, the connection with the Tyr124 amino acid elucidated how the enzyme activity was inhibited, providing insight into the binding mechanism in the PAS region.

The interactions of Trp86, Tyr124, and Tyr337 residues with the ligand's pyrrole ring indicated that the NH group of the pyrrole ring and the ring itself significantly influenced inhibitory activity. Consequently, it is believed that the pyrrole ring is a valuable pharmacophore group. This, along with its bioisosteres or analogs, may contribute to the development of more effective AChE inhibitors.

2.8 | DFT analysis results

2.8.1 | The theoretical geometry analysis

Using DFT/B3LYP/6-311++G(d,p), optimized molecular structures with total energy values of compounds **5a**–**5m** and **8a**–**8s** are shown in Supporting Information S1: Figure S2 and S3. The total energy values (Figure S2) for the compounds **5a**–**5m** obey the following order: **5j** < **5m** < **5h** < **5b** < **5l** < **5i** < **5f** < **5k** < **5e** < **5a** < **5g** < **5d** < **5c**. The total energy values (Supporting Information S1: Figure S3) for the compounds **8a**–**8s** obey the following order: **8o** < **8b** < **8r** < **8s** < **8d** < **8l** < **8k** < **8g** < **8q** < **8p** < **8j** < **8i** < **8h** < **8f** < **8c** < **8e** < **8a** < **8m** < **8n**. Compounds with lower total energy values can be deemed to have a more stable structure, according to the computed total energy values of molecular structures.

2.8.2 | Dipole moments

The dipole moment is a measure of the polarity of the molecule. Furthermore, the value of the dipole moment was calculated at the DFT/B3LYP/6-311++G(d,p) level using Equation (1), and the results are presented in Tables 4 and 5. From the group of compounds **5a**–**5m**, the dipole moment of molecule **5m** suggests that it is relatively the more polarized one, while molecule **5b** is the less polarized one. From the group compounds **8a**–**8s**, the dipole moment of molecule **8p** suggests that it is relatively the more polarized one, while molecule **8l** is the less polarized one.

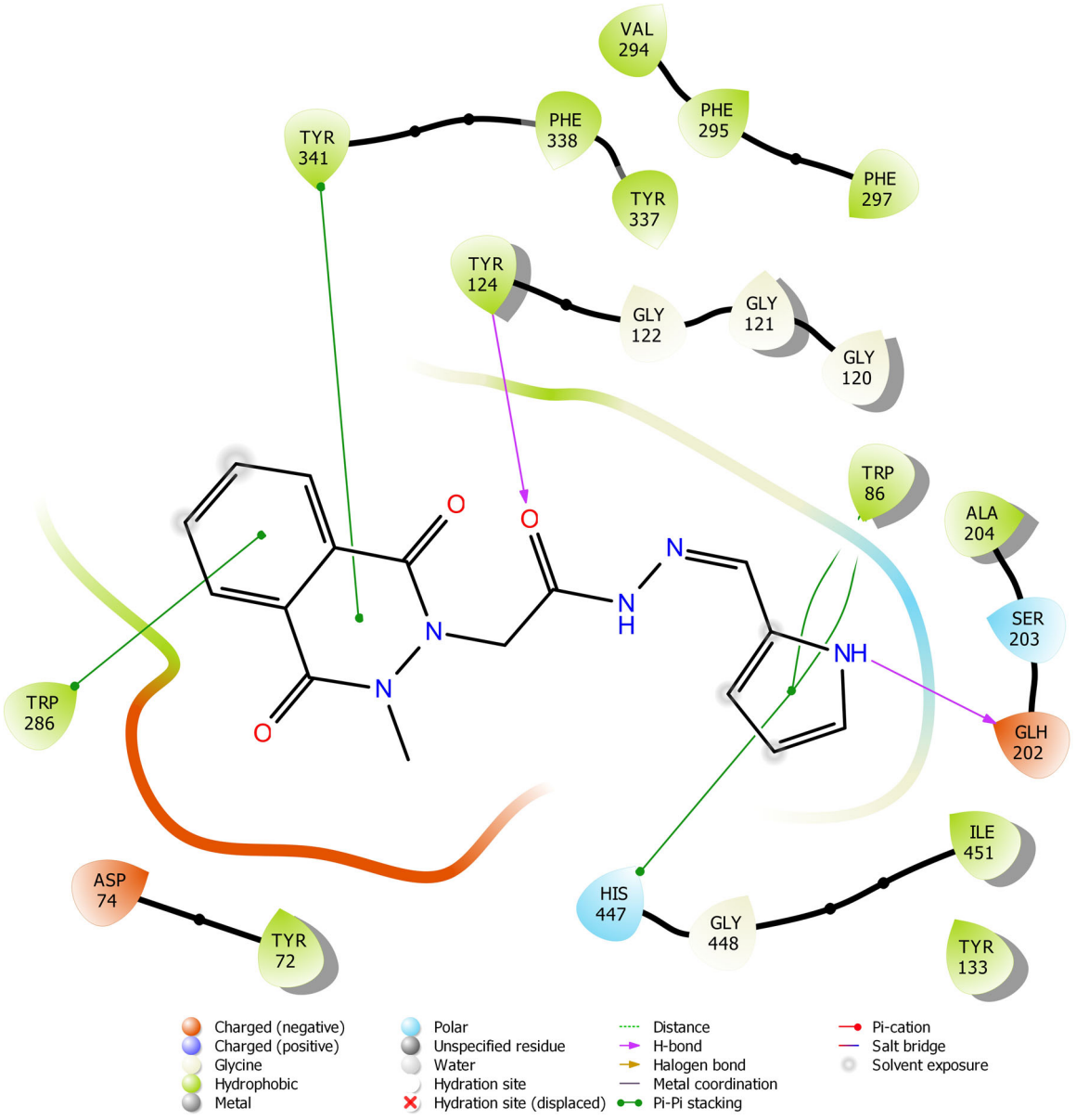

FIGURE 6 Compound **8n**'s two-dimensional pose and interactions at the acetylcholinesterase (AChE) active site.

2.8.3 | Frontier molecular orbitals

HOMO–LUMO energy values, also known as frontier molecular orbital energies, play a crucial role in determining various reactivity parameters of chemical structures, particularly in modeling studies involving molecular groups derived from various substituents. It is important to note that a high HOMO energy value indicates a molecule's capacity to donate electrons, while a low LUMO energy value signifies a chemical structure's ability to accept electrons.[36] The HOMO–LUMO energy gap values are essential for identifying molecular groups that tend to be nucleophilic or electrophilic. Additionally, the HOMO–LUMO (E) energy gap provides information about the stability and reactivity of molecular systems; narrower energy gaps indicate less stability and greater reactivity. In Table 6, the calculated HOMO and LUMO energy gap values for compounds **5a–5m** are presented. Compound **5k** has the smallest energy gap (ΔE) with a value of 0.0619 Ha, indicating higher reactivity and lower stability. Conversely, compounds **5a** and **5j** have the largest energy gap (ΔE) with a value of 0.0871 Ha, suggesting lower reactivity and greater stability. The HOMO-LUMO orbital diagrams of **5a–5m** compounds are shown in Supporting Information S1: Figure S4.

For specific compounds, **5j** exhibits a low I value (ionization potential), and **5k** has a high A value (electron affinity) associated with HOMO and LUMO energy. Therefore, compound **5j** has a nucleophilic character, while compound **5k** exhibits an electrophilic character relative to the others.

Electronegativity (χ) is the tendency of an atom to attract shared electrons or electron density to itself. Higher electronegativity values indicate stronger electron-attracting capabilities. In contrast, electropositivity measures a molecule's ability to donate valence electrons.

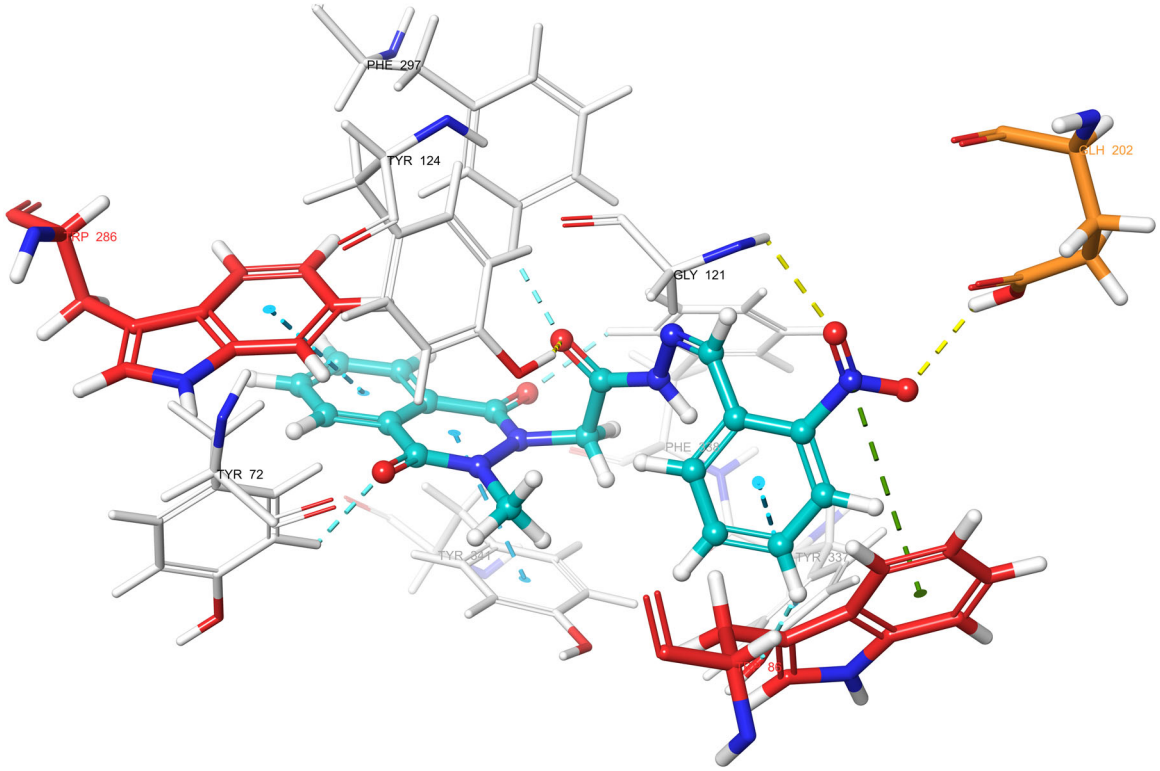

FIGURE 7 Compound **8p**'s three-dimensional pose and interactions at the acetylcholinesterase (AChE) active site.

The electronegativity (χ) values for the **5a–5m** compounds are in decreasing order: **5k** > **5g** > **5l** > **5f** > **5c** > **5h** > **5i** > **5m** > **5d** > **5b** > **5e** > **5a** > **5j**. The electrophilic character (ω) values follow the decreasing order: **5k** > **5g** > **5l** > **5f** > **5c** > **5h** > **5m** > **5i** > **5d** > **5b** > **5e** > **5j** > **5a**. Compound **5k**, with χ = 0.2436 Ha and ω = 0.9602 Ha, exhibits higher electronegativity and a better electrophilic character than the others.

Furthermore, the chemical hardness-softness values (η, S) are effective in determining the intramolecular charge transfer of molecular structures. The compound with a high S (softness) and low η (hardness) value is **5k**, indicating its characteristics in charge transfer within the molecular structure.

Table 7 presents the calculated HOMO and LUMO energy gap values for the **8a–8s** compounds. Among these compounds, **8i** has the smallest energy gap (Δ*E*) with a value of 0.0680 Ha, indicating higher reactivity and lower stability. In contrast, compounds **8f** and **8h** have the largest energy gap (Δ*E*) with a value of 0.0908 Ha, suggesting lower reactivity and greater stability. The HOMO–LUMO orbital diagrams of **8a–8s** compounds are shown in Supporting Information S1: Figure S5.

Among the specified compounds, **8m** has a low ionization potential (I) value, while **8i** exhibits a high electron affinity (A) value associated with HOMO and LUMO energy. Consequently, compound **8m** displays a nucleophilic character, whereas compound **8i** has a more pronounced electrophilic character compared with the others.

Electronegativity (χ) measures the tendency of an atom to attract shared electrons or electron density to itself. Higher electronegativity values indicate a stronger electron-attracting capability. Conversely, electro-positivity represents a molecule's ability to donate valence electrons. The electronegativity (χ) values for the **8a–8s** compounds are in decreasing order: **8i** > **8j** > **8k** > **8q** > **8a** > **8r** > **8b** > **8e** > **8p** > **8o** > **8n** > **8s** > **8d** > **8c** > **8l** > **8g** > **8f** > **8m** > **8h**. The electrophilic character (ω) values follow the decreasing order: **8i** > **8j** > **8k** > **8a** > **8q** > **8p** > **8b** > **8e** > **8r** > **8s** > **8o** > **8n** > **8d** > **8c** > **8l** > **8g** > **8m** > **8f** > **8h**. Compound **8i**, with χ = 0.2422 Ha and ω = 0.8627 Ha, exhibits higher electronegativity and a better electrophilic character than the others.

The chemical hardness-softness values (η, S) are effective in determining the intramolecular charge transfer of molecular structures. Compound **8i**, with its high S (softness) and low η (hardness) values, demonstrates its charge transfer characteristics within the molecular structure.

2.8.4 | Molecular electrostatic potentials (MEPs) values

The MEP represents the force acting on a positive test charge (such as a proton) when placed within the electron and nuclear charge cloud created by a molecule. It provides valuable insights into a molecule's reactivity toward positively or negatively charged reactants, even without affecting the molecule's charge distribution. In the visual representation of MEP, attractive potential regions are typically depicted in red, while repulsive potential regions are shown

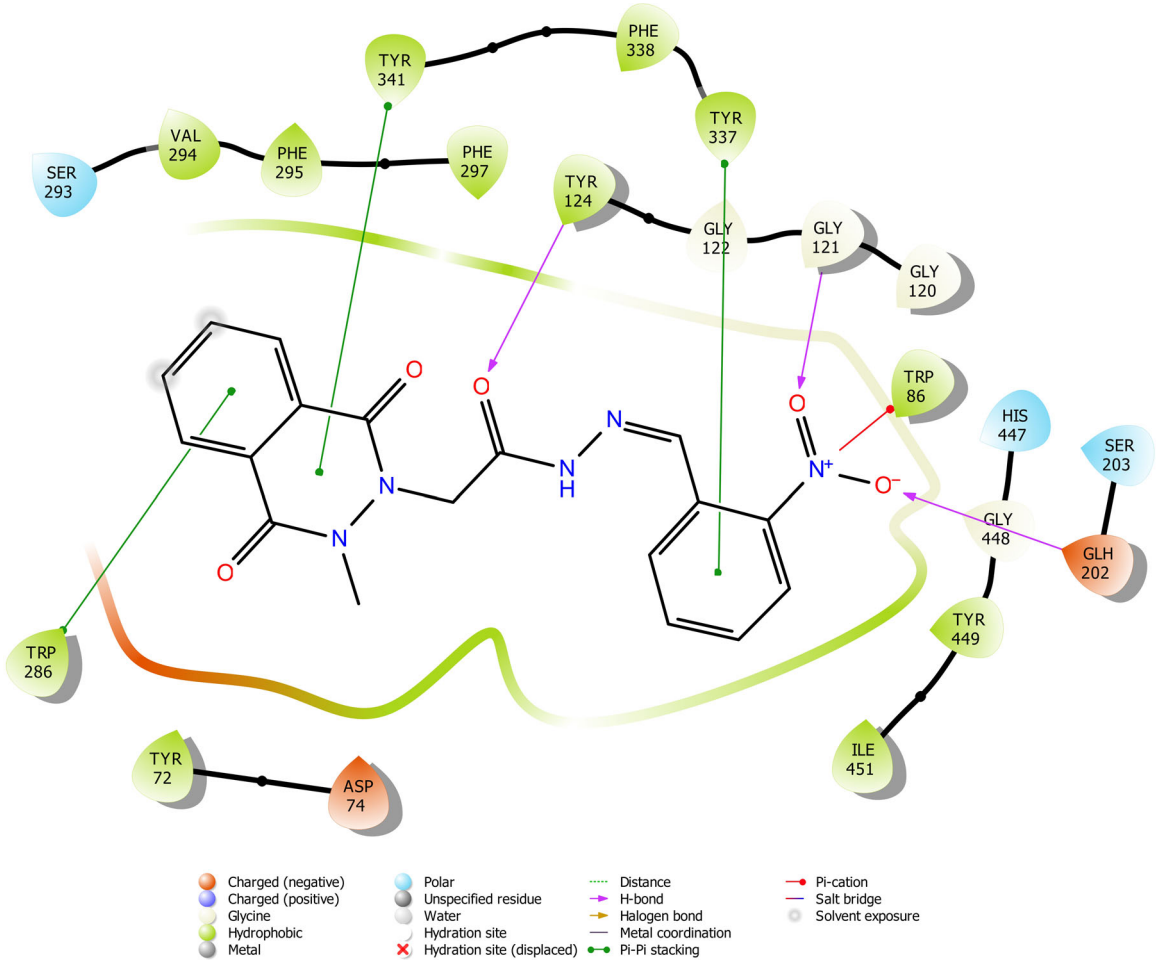

FIGURE 8 Compound **8p**'s two-dimensional pose and interactions at the acetylcholinesterase (AChE) active site.

in blue. For the **5a–5m** and **8a–8s** compounds, the MEP is illustrated in Supporting Information S1: Figures S6 and S7, respectively.

3 | CONCLUSIONS

The development of targeted phthalazine-1,4-dione AChE inhibitors as potential AD treatment candidates involved the synthesis of 32 compounds in a multistage process. In the first phase of synthesis, 2-bromoacetophenone compounds were synthesized from acetophenone derivatives in acetic acid. The reaction temperature was controlled, and various solvents were tested in subsequent stages of synthesis. The compounds were characterized using various techniques, such as ^{1}H NMR, ^{13}C NMR, and mass spectrometry, to confirm their identities.

The biological activity of these compounds against AChE and BChE was evaluated in vitro, and it was found that 13 compounds inhibited AChE by more than 50%, with no effect on BChE. Further analysis revealed that specific compounds, including **8m**, **8n**, and **8p**, exhibited exceptional activity similar to donepezil, explaining their significant inhibitory effect against AChE. Molecular docking studies showed that these active compounds bind to the AChE enzyme in a position similar to donepezil.

The enzyme kinetic studies, particularly focusing on compound **8n**, demonstrated mixed inhibition activity against AChE, as evidenced by intersecting Lineweaver–Burk curves. This finding suggests a combination of competitive and noncompetitive characteristics in the inhibitory mechanism. Additionally, the effective derivatives **8m**, **8n**, and **8p** exhibited notable permeability through the BBB in in vitro PAMPA tests, underscoring their potential for central nervous system targeting in the pursuit of effective AD therapeutics.

Molecular dynamics simulation (MDS) analysis of the **8n**-AChE enzyme complexes demonstrated that the protein–ligand system remained stable throughout the simulation, indicating sustained complex stability. Additionally, the chemical reactivity features of the targeted compounds were investigated using DFT, and compounds like **8m**, **8n**, and **8p** were found to have high energy gaps, signifying their stability.

In conclusion, the development of these targeted compounds represents a significant advancement in the search for a potential cure for AD. The process involved meticulous synthesis, comprehensive characterization, extensive biological activity, and molecular docking studies. The stability of the protein–ligand system and the high energy gap of these compounds offer promising prospects for their therapeutic potential. However, further research and testing are needed to determine their safety and efficacy in AD treatment.

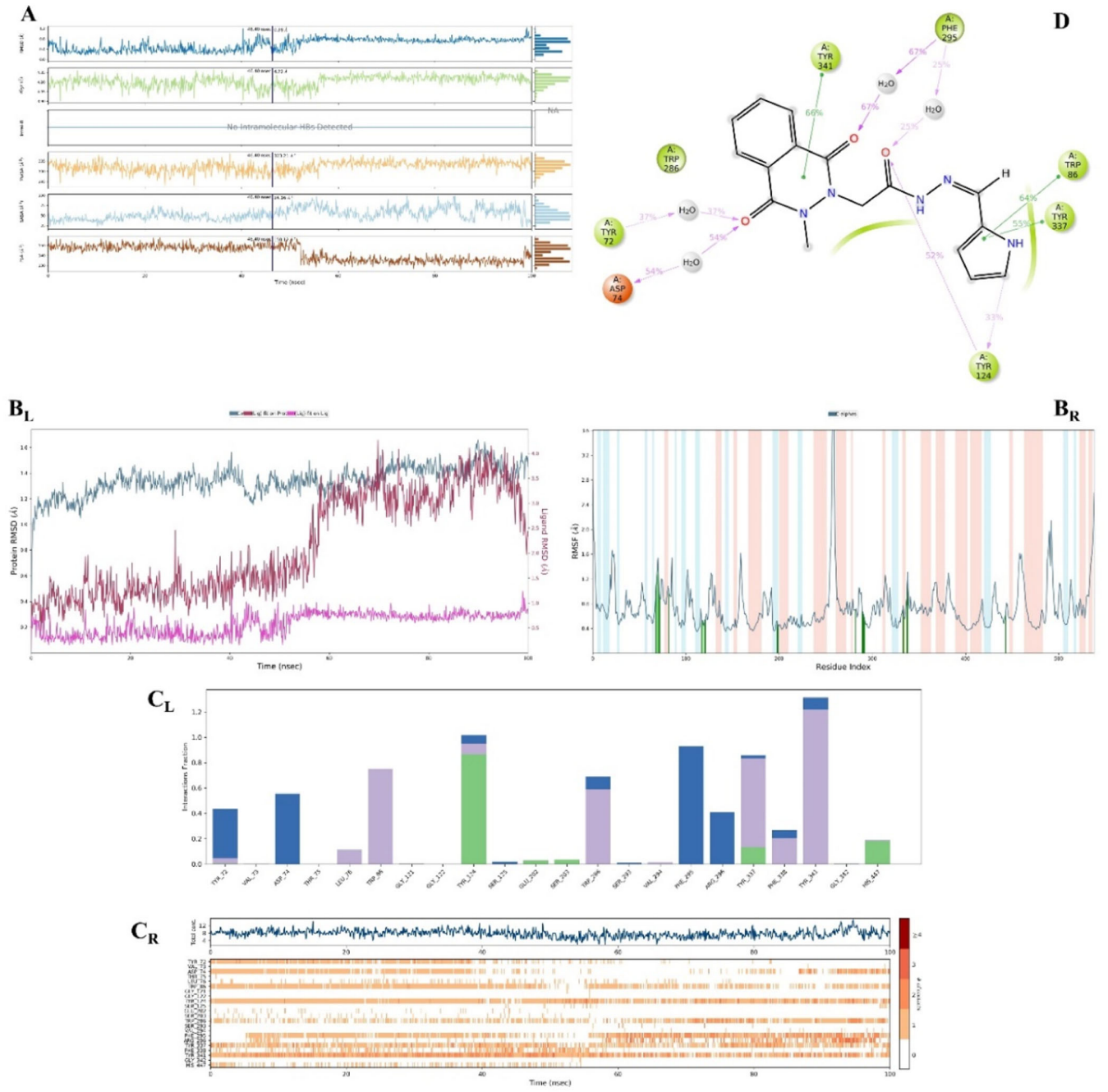

FIGURE 9 Plots of the molecular dynamics simulation (MDS) results for the compound **8n**–acetylcholinesterase (AChE) enzyme complex. Stability properties: (a) Rg, (B_L) RMSD, and (B_R) RMSF plots. Interaction properties: (C_L) interaction fraction–residue diagram, (C_R) total connections–residues–time plot, and (d) two-dimensional (2D) interaction pose with the connection strength (cut off of 0.2) at the active region. RMSD, the root mean square deviation; RMSF, root mean square fluctuation; Rg, the radius of gyration.

4 | EXPERIMENTAL

4.1 | Chemistry

4.1.1 | General

All chemicals were purchased from Sigma-Aldrich Chemical Co (Sigma-Aldrich Corp.) and Merck Chemicals (Merck KGaA). All melting points (m.p.) were determined using an MP90 digital melting point apparatus (Mettler Toledo) and were uncorrected. Reactions were monitored by TLC using Silica Gel 60 F254 TLC plates (Merck KGaA). ^{1}H NMR and ^{13}C NMR spectral analyses were conducted using a Bruker digital FT-NMR spectrometer (Bruker Bioscience) set to 300 and 75 MHz, respectively. Samples were prepared in DMSO-d6 for these NMR analyses. Mass analysis was performed using a Shimadzu 8040 HRMS system (Shimadzu).

The InChI codes of the investigated compounds are provided as Supporting Information.

TABLE 4 The values of the electric dipole moment of the **5a–5m** compounds.

Compounds	μ_x (Debye)	μ_y (Debye)	μ_z (Debye)	μ_{tot} (Debye)
5a	1.0367	−0.2334	1.8139	2.1022
5b	−0.8184	−1.6037	0.9899	2.0547
5c	3.3083	0.0400	1.8024	3.7676
5d	0.8913	2.5908	1.8443	3.3027
5e	4.0868	−1.0056	3.3927	5.4058
5f	4.2090	−0.8374	0.3241	4.3037
5g	−1.9770	0.3741	1.9984	2.8358
5h	0.9349	−0.5989	3.4462	3.6206
5i	0.8349	1.8583	1.1942	2.3615
5j	0.5018	0.3469	3.1440	3.2027
5k	3.7223	0.0641	1.7927	4.1320
5l	−1.0017	2.8035	1.2119	3.2143
5m	−4.9833	3.0140	1.1228	5.9312

TABLE 5 The values of the electric dipole moment of the **8a–8s** compounds.

Compounds	μ_x (Debye)	μ_y (Debye)	μ_z (Debye)	μ_{tot} (Debye)
8a	−0.9979	−1.4380	0.2875	1.7738
8b	−2.9151	−1.0340	0.7208	3.1759
8c	−2.6796	−0.9700	0.7225	2.9399
8d	−2.9286	−1.0037	0.7107	3.1763
8e	−0.2777	−1.6822	0.1737	1.7138
8f	2.1904	5.8979	1.7858	6.5400
8g	3.4774	−4.8836	1.7627	6.2489
8h	−1.0543	−6.7076	2.2224	7.1444
8i	−3.9996	1.6307	0.0805	4.3200
8j	−3.8984	1.4202	0.3147	4.1609
8k	−3.5518	−5.6367	1.4345	6.8151
8l	−0.6658	−1.0344	0.1498	1.2393
8m	−1.5115	5.7174	1.2335	6.0411
8n	0.0029	3.3068	1.5390	3.6474
8o	−0.9231	−6.0696	1.7005	6.3706
8p	−4.3017	5.7477	3.4913	7.9831
8q	−3.5704	−2.1847	3.2612	5.3062
8r	0.9328	1.7732	0.6583	2.1090
8s	1.1836	−0.2584	2.6022	2.8704

4.1.2 | General method for the synthesis of 2-bromoacetophenone derivatives (2)

Acetophenone derivatives (1) (20 mmol) were mixed with acetic acid (50 mL) and hydrobromic acid (2 mL) in a flask. Bromine (1 equivalent) was slowly added drop by drop using a pipette at 0°C with stirring. The mixture was then stirred at room temperature for 2–8 h while monitoring the reaction with TLC and CMS. After completion, the mixture was gradually added to ice water, and the resulting precipitate was filtered and recrystallized with ethanol.

4.1.3 | General method for the synthesis of 2-methyl-2,3-dihydrophthalazine-1,4-dione (4)

Methylhydrazine (1.03 g, 22.28 mmol) was added to a solution of phthalic anhydride (3 g, 20.25 mmol) in acetic acid (50 mL) at room temperature. The mixture was stirred for 5 h at 125°C. TLC and CMS were used to keep track of the response. The liquid was allowed to cool when the reaction was finished. The cooling reaction was poured into iced water, and the product precipitated as a white solid. The resulting product was filtered, washed with water, and dried (m. p. 231–232°C, yield 88%).

4.1.4 | General procedure for the synthesis of 2-methyl-3-(2-oxo-2-phenylethyl)−2,3-dihydrophthalazine-1,4-dione derivatives (5a–5m)

Sodium hydride (NaH, 1.56 mmol, 0.037 g) was added slowly to a solution of 2-methyl-2,3-dihydrophthalazine-1,4-dione (**4**) (1.42 mmol, 0.25 g) in dimethylformamide (DMF) (10 mL). After the mixture was stirred for 40 min at room temperature, 2-bromoacetophenone derivatives (**2**) (1.42 mmol) were dissolved in DMF (2 mL) and added dropwise to this mixture. The mixture was stirred for 2 days at room temperature. TLC and CMS were used to monitor the reaction. After the reaction was complete, the mixture was poured into ice water, and the product was precipitated. The resulting product is filtered, washed with water, and dried (72%–89%).

2-[2-(4-Fluorophenyl)−2-oxoethyl]-3-methyl-2,3-dihydrophthalazine-1,4-dione (**5a**): Solid white crystals, yield: 86%, m.p. 144–145°C, ^{1}H NMR (300 MHz, DMSO-d_6, ppm) δ: 3.47 (s, 3H, N–$\underline{CH_3}$), 5.79 (s, 2H, N–$\underline{CH_2}$), 7.43 (t, J = 8.86 Hz, 2H, Ar-H), 7.96 (d, J = 7.63 Hz, 1H, Ar-H), 8.01 (d, J = 7.21 Hz, 1H, Ar-H), 8.08 (d, J = 7.37 Hz, 1H, Ar-H), 8.11–8.16 (m, 2H, Ar-H), 8.27 (d, J = 7.45 Hz, 1H, Ar-H). ^{13}C NMR (75 MHz, DMSO-d_6, ppm) δ: 38.86 (N–$\underline{CH_3}$), 68.87 (N–$\underline{CH_2}$), 116.38, 123.82, 124.14, 126.94, 128.74, 131.27, 133.18, 133.91, 148.19, 158.02, 164.13, 167.47, 192.72. HRMS (*m/z*) $[M+H]^+$: For $C_{17}H_{13}FN_2O_3$ calculated: 313.0983, found: 313.0994.

2-[2-(4-Chlorophenyl)-2-oxoethyl]-3-methyl-2,3-dihydrophthalazine-1,4-dione (**5b**): Solid white crystals, yield: 79%, m.p. 157–158°C.^{1}H NMR (300 MHz, DMSO-d_6, ppm) δ: 3.46 (s, 3H, N–$\underline{CH_3}$), 5.78 (s, 2H, N–$\underline{CH_2}$), 7.66 (d, J = 8.63 Hz, 2H, Ar-H), 7.95 (d, J = 7.52 Hz, 1H, Ar-H) 8.00

TABLE 6 Some reactivity parameters of the compounds **5a–5m**.

Compounds	E_{HOMO} (Ha)	E_{LUMO} (Ha)	ΔE (Ha)	I (Ha)	A (Ha)	χ (Ha)	η (Ha)	S (Ha^{-1})	μ (Ha)	ω (Ha)
5a	−0.2750	−0.1879	0.0871	0.2750	0.1879	0.2314	0.0453	11.0375	−0.2314	0.5910
5b	−0.2759	−0.1929	0.0830	0.2759	0.1929	0.2344	0.0415	12.0482	−0.2344	0.6620
5c	−0.2746	−0.2010	0.0736	0.2746	0.2010	0.2378	0.0368	13.5869	−0.2378	0.7683
5d	−0.2748	−0.1969	0.0779	0.2748	0.1969	0.2358	0.0389	12.8535	−0.2358	0.7147
5e	−0.2746	−0.1882	0.0864	0.2746	0.1882	0.2314	0.0432	11.5741	−0.2314	0.6197
5f	−0.2749	−0.2033	0.0716	0.2749	0.2033	0.2391	0.0358	13.9665	−0.2391	0.7984
5g	−0.2748	−0.2100	0.0648	0.2748	0.2100	0.2424	0.0324	15.4321	−0.2424	0.9067
5h	−0.2749	−0.1997	0.0752	0.2749	0.1997	0.2373	0.0376	13.2979	−0.2373	0.7488
5i	−0.2757	−0.1981	0.0776	0.2757	0.1981	0.2369	0.0388	12.8866	−0.2369	0.7232
5j	−0.2744	−0.1873	0.0871	0.2744	0.1873	0.2308	0.0435	11.4942	−0.2308	0.6123
5k	−0.2746	−0.2127	0.0619	0.2746	0.2127	0.2436	0.0309	16.1812	−0.2436	0.9602
5l	−0.2747	−0.2073	0.0674	0.2747	0.2073	0.2410	0.0337	14.8368	−0.2410	0.8617
5m	−0.2746	−0.1979	0.0767	0.2746	0.1979	0.2362	0.0383	13.0548	−0.2362	0.7283

TABLE 7 Some reactivity parameters of the compounds **8a–8s**.

Compounds	E_{HOMO} (Ha)	E_{LUMO} (Ha)	ΔE (Ha)	I (Ha)	A (Ha)	χ (Ha)	η (Ha)	S (Ha^{-1})	μ (Ha)	ω (Ha)
8a	−0.2728	−0.1900	0.0828	0.2728	0.1900	0.2314	0.0414	12.0773	−0.2314	0.6467
8b	−0.2730	−0.1877	0.0853	0.2730	0.1877	0.2303	0.0426	11.7371	−0.2303	0.6225
8c	−0.2731	−0.1828	0.0903	0.2731	0.1828	0.2279	0.0451	11.0865	−0.2279	0.5758
8d	−0.2732	−0.1830	0.0902	0.2732	0.1830	0.2281	0.0451	11.0865	−0.2281	0.5768
8e	−0.2729	−0.1875	0.0854	0.2729	0.1875	0.2302	0.0427	11.7096	−0.2302	0.6205
8f	−0.2726	−0.1818	0.0908	0.2726	0.1818	0.2272	0.0454	11.0132	−0.2272	0.5685
8g	−0.2725	−0.1823	0.0902	0.2725	0.1823	0.2274	0.0451	11.0865	−0.2274	0.5733
8h	−0.2724	−0.1816	0.0908	0.2724	0.1816	0.2270	0.0454	11.0132	−0.2270	0.5675
8i	−0.2762	−0.2082	0.0680	0.2762	0.2082	0.2422	0.0340	14.7059	−0.2422	0.8627
8j	−0.2725	−0.2041	0.0684	0.2725	0.2041	0.2383	0.0342	14.6199	−0.2383	0.8302
8k	−0.2723	−0.2022	0.0701	0.2723	0.2022	0.2372	0.0350	14.2857	−0.2372	0.8038
8l	−0.2728	−0.1825	0.0903	0.2728	0.1825	0.2276	0.0451	11.0865	−0.2276	0.5743
8m	−0.2722	−0.1818	0.0904	0.2722	0.1818	0.2270	0.0452	11.0619	−0.2270	0.5700
8n	−0.2735	−0.1842	0.0893	0.2735	0.1842	0.2288	0.0446	11.2108	−0.2288	0.5869
8o	−0.2736	−0.1843	0.0893	0.2736	0.1843	0.2289	0.0446	11.2108	−0.2289	0.5874
8p	−0.2723	−0.1881	0.0842	0.2723	0.1881	0.2302	0.0421	11.8765	−0.2302	0.6294
8q	−0.2737	−0.1894	0.0843	0.2737	0.1894	0.2315	0.0421	11.8765	−0.2315	0.6365
8r	−0.2754	−0.1855	0.0899	0.2754	0.1855	0.2304	0.0449	11.1359	−0.2304	0.5911
8s	−0.2732	−0.1844	0.0888	0.2732	0.1844	0.2288	0.0444	11.2613	−0.2288	0.5895

(d, J = 7.16 Hz, 1H, Ar-H), 8.04 (d, J = 1.93 Hz, 1H, Ar-H), 8.05–8.08 (m, 2H, Ar-H), 8.26 (d, J = 6.98 Hz, 1H, Ar-H). ^{13}C NMR (75 MHz, DMSO-d_6, ppm) δ: 38.86 (N–$\underline{CH_3}$), 68.95 (N–$\underline{CH_2}$), 123.82, 124.12, 126.95, 128.75, 129.57, 130.20, 133.20, 133.47, 133.94, 139.22, 148.16, 158.02, 193.24. HRMS (m/z) $[M+H]^+$: For $C_{17}H_{13}ClN_2O_3$ calculated: 329.0687, found: 329.0691.

2-Methyl-3-(2-oxo-2-phenylethyl)-2,3-dihydrophthalazine-1,4-dione (**5c**): Solid white crystals, yield: 83%, m.p. 153–154°C. ^{1}H NMR

(300 MHz, DMSO-d_6, ppm) δ: 3.47 (s, 3H, N–$\underline{CH_3}$), 5.81 (s, 2H, N–$\underline{CH_2}$), 7.60 (t, J = 7.56 Hz, 2H, Ar-H), 7.72 (t, J = 7.39 Hz, 1H, Ar-H), 7.91–7.99 (m, 2H, Ar-H), 8.01–8.10 (m, 3H, Ar-H), 8.27 (d, J = 7.49 Hz, 1H, Ar-H). ^{13}C NMR (75 MHz, DMSO-d_6, ppm) δ: 38.81 (N–$\underline{CH_3}$), 68.97 (N–$\underline{CH_2}$), 123.82, 124.16, 126.92, 128.21, 128.73, 129.42, 133.14, 133.88, 134.34, 134.78, 148.21, 158.01, 194.02. HRMS (m/z) $[M+H]^+$: For $C_{17}H_{14}N_2O_3$ calculated: 295.1077, found: 295.1073.

2-Methyl-3-[2-oxo-2-(*p*-tolyl)ethyl]-2,3-dihydrophthalazine-1,4-dione (**5d**): Solid white crystals, yield: 75%, m.p. 155–156°C. ^{1}H NMR (300 MHz, DMSO-d_6, ppm) δ: 2.41 (s, 3H, Ph–$\underline{CH_3}$), 3.46 (s, 3H, N–$\underline{CH_3}$), 5.77 (s, 2H, N–$\underline{CH_2}$), 7.39 (d, J = 7.78 Hz, 2H, Ar-H), 7.92–7.97 (m, 3H, Ar-H) 8.00 (d, J = 7.19 Hz, 1H, Ar-H), 8.08 (d, J = 7.89 Hz, 1H, Ar-H), 8.27 (d, J = 7.74 Hz, 1H, Ar-H). ^{13}C NMR (75 MHz, DMSO-d_6, ppm) δ: 21.73 (Ph–$\underline{CH_3}$), 38.86 (N–$\underline{CH_3}$), 68.86 (N–$\underline{CH_2}$), 123.83, 124.18, 126.92, 128.31, 128.73, 129.93, 132.27, 133.14, 133.88, 144.85, 148.25, 158.01, 193.44. HRMS (m/z) $[M+H]^+$: For $C_{18}H_{16}N_2O_3$ calculated: 309.1234, found: 309.1247.

2-[2-(4-Methoxyphenyl)-2-oxoethyl]-3-methyl-2,3-dihydrophthalazine-1,4-dione (**5e**): Solid white crystals, yield: 86%, m.p. 151–152°C. ^{1}H NMR (300 MHz, DMSO-d_6, ppm) δ: 3.47 (s, 3H, N–$\underline{CH_3}$), 3.87 (s, 3H, Ph–O$\underline{CH_3}$), 5.75 (s, 2H, N–$\underline{CH_2}$), 7.11 (d, J = 8.94 Hz, 2H, Ar-H), 7.95 (d, J = 7.63 Hz, 2H, Ar-H) 7.99–8.01 (m, 2H, Ar-H), 8.02–8.04 (m, 1H, Ar-H), 8.08 (d, J = 7.12 Hz, 1H, Ar-H), 8.27 (d, J = 7.03 Hz, 1H, Ar-H). ^{13}C NMR (75 MHz, DMSO-d_6, ppm) δ: 38.85 (N–$\underline{CH_3}$), 56.11 (Ph–O$\underline{CH_3}$), 68.67 (N–$\underline{CH_2}$), 114.63, 123.86, 124.23, 126.92, 127.61, 128.74, 130.60, 133.14, 133.89, 148.33, 158.03, 164.05, 192.21. HRMS (m/z) $[M+H]^+$: For $C_{18}H_{16}N_2O_4$ calculated: 325.1183, found: 325.1199.

2-Methyl-3-[2-(4-nitrophenyl)-2-oxoethyl]-2,3-dihydrophthalazine-1,4-dione (**5f**): Solid white crystals, yield: 89%, m.p. 221–222°C. ^{1}H NMR (300 MHz, DMSO-d_6, ppm) δ: 3.47 (s, 3H, N–$\underline{CH_3}$), 5.84 (s, 2H, N–$\underline{CH_2}$), 7.93–8.03 (m, 2H, Ar-H), 8.08 (d, J = 7.15 Hz, 1H, Ar-H), 8.27 (d, J = 8.75 Hz, 3H, Ar-H) 8.40 (d, J = 8.78 Hz, 2H, Ar-H). ^{13}C NMR (75 MHz, DMSO-d_6, ppm) δ: 38.83 (N–$\underline{CH_3}$), 69.30 (N–$\underline{CH_2}$), 123.81, 124.04, 124.52, 126.99, 128.76, 129.78, 133.28, 133.99, 139.49, 148.06, 150.72, 158.03, 193.78. HRMS (m/z) $[M+H]^+$: For $C_{17}H_{13}N_3O_5$ calculated: 340.0928, found: 340.0930.

4-[2-(3-Methyl-1,4-dioxo-3,4-dihydrophthalazin-2(1*H*)-yl)acetyl] benzonitrile (**5g**): Solid white crystals, yield: 72%, m.p. 225–226°C. ^{1}H NMR (300 MHz, DMSO-d$_6$, ppm) δ: 3.46 (s, 3H, N–$\underline{CH_3}$), 5.82 (s, 2H, N–$\underline{CH_2}$), 7.91–8.02 (m, 2H, Ar-H), 8.08 (d, J = 8.52 Hz, 3H, Ar-H), 8.18 (d, J = 8.61 Hz, 2H, Ar-H) 8.26 (d, J = 7.42 Hz, 1H, Ar-H). ^{13}C NMR (75 MHz, DMSO-d$_6$, ppm) δ: 38.80 (N–$\underline{CH_3}$), 69.21 (N–$\underline{CH_2}$), 116.19, 118.54, 123.79, 124.05, 128.76, 128.93, 133.25, 133.46, 133.96, 138.03, 148.06, 158.02, 193.87. HRMS (m/z) $[M+H]^+$: For $C_{18}H_{13}N_3O_3$ calculated: 320.1030, found: 320.1031.

2-[2-(3-Chlorophenyl)-2-oxoethyl]-3-methyl-2,3-dihydrophthalazine-1,4-dione (**5h**): Solid white crystals, yield: 74%, m.p. 129–130°C. ^{1}H NMR (300 MHz, DMSO-d$_6$, ppm) δ: 3.47 (s, 3H, N–$\underline{CH_3}$), 5.80 (s, 2H, N–$\underline{CH_2}$), 7.62 (t, J = 7.89 Hz, 1H, Ar-H), 7.78 (d, J = 8.02 Hz, 1H, Ar-H) 7.92 (d, J = 7.31 Hz, 1H, Ar-H), 7.96–8.01 (m, 2H, Ar-H), 8.04–8.09 (m, 2H, Ar-H), 8.26 (d, J = 7.49 Hz, 1H, Ar-H). ^{13}C NMR (75 MHz, DMSO-d$_6$, ppm) δ: 38.85 (N–$\underline{CH_3}$), 69.07 (N–$\underline{CH_2}$), 123.81, 124.11, 126.95, 127.94, 128.76, 131.46, 133.21, 133.93, 134.05, 134.32, 136.58, 148.10, 158.02, 193.24. HRMS (–) $[M+H]^+$: For $C_{17}H_{13}ClN_2O_3$ calculated: 329.0687, found: 329.0713.

2-Methyl-3-[2-(3-nitrophenyl)-2-oxoethyl]-2,3-dihydrophthalazine-1,4-dione (**5i**): Solid white crystals, yield: 78%, m.p. 134–135°C. ^{1}H NMR (300 MHz, DMSO-d_6, ppm) δ: 3.46 (s, 3H, N–$\underline{CH_3}$), 5.87 (s, 2H, N–$\underline{CH_2}$), 7.89 (t, J = 8.00 Hz, 1H, Ar-H), 7.93–8.01 (m, 2H, Ar-H), 8.07 (d, J = 7.40 Hz, 1H, Ar-H), 8.25 (d, J = 7.24 Hz, 1H, Ar-H), 8.46 (d, J = 8.05 Hz, 1H, Ar-H), 8.53 (d, J = 8.23 Hz, 1H, Ar-H), 8.72 (s, 1H, Ar-H). ^{13}C NMR (75 MHz, DMSO-d_6, ppm) δ: 38.82 (N–$\underline{CH_3}$), 69.19 (N–$\underline{CH_2}$), 122.72, 123.79, 124.04, 126.97, 128.48, 128.75, 131.29, 133.24, 133.95, 134.53, 135.96, 148.06, 148.54, 158.02, 193.08. HRMS (m/z) $[M+H]^+$: For $C_{17}H_{13}N_3O_5$ calculated: 340.0928, found: 340.0958.

2-[2-(3,4-Dichlorophenyl)-2-oxoethyl]-3-methyl-2,3-dihydrophthalazine-1,4-dione (**5j**): Solid white crystals, yield: 87%, m.p. 161–162°C. ^{1}H NMR (300 MHz, DMSO-d$_6$, ppm) δ: 3.47 (s, 3H, N–$\underline{CH_3}$), 5.79 (s, 2H, N–$\underline{CH_2}$), 7.86 (d, J = 8.40 Hz, 1H, Ar-H), 7.94 (d, J = 7.63 Hz, 1H, Ar-H), 7.97–8.01 (m, 2H, Ar-H), 8.06 (d, J = 7.20 Hz, 1H, Ar-H). 8.24–8.27 (m, 2H, Ar-H). ^{13}C NMR (75 MHz, DMSO-d$_6$, ppm) δ: 38.85 (N–$\underline{CH_3}$), 69.01 (N–$\underline{CH_2}$), 123.79, 124.07, 126.96, 128.33, 128.75, 130.24, 131.81, 132.50, 133.21, 133.93, 134.88, 137.14, 148.05, 158.02, 192.57. HRMS (*m/z*) $[M+H]^+$: For $C_{17}H_{12}Cl_2N_2O_3$ calculated: 349.0141, found: 349.0177.

Synthesis of 2-methyl-3-[2-(naphthalen-2-yl)-2-oxoethyl]-2,3-dihydrophthalazine-1,4-dione (**5k**): Solid white crystals, yield: 82%, m.p. 149–150°C. ^{1}H NMR (300 MHz, DMSO-d_6, ppm) δ: 3.46 (s, 3H, N–$\underline{CH_3}$), 5.93 (s, 2H, N–$\underline{CH_2}$), 7.62–7.73 (m, 2H, Ar-H), 7.92 (d, J = 7.41 Hz, 1H, Ar-H), 7.96 (d, J = 1.86 Hz, 1H, Ar-H), 7.99 (d, J = 1.74 Hz, 1H, Ar-H), 8.01–8.04 (m, 1H, Ar-H), 8.06–8.12 (m, 2H, Ar-H), 8.17 (d, J = 7.60 Hz, 1H, Ar-H), 8.26 (d, J = 7.56 Hz, 1H, Ar-H), 8.79 (s, 1H, Ar-H). ^{13}C NMR (75 MHz, DMSO-d_6, ppm) δ: 38.83 (N–$\underline{CH_3}$), 69.02 (N–$\underline{CH_2}$), 123.66, 123.87, 124.21, 126.94, 127.62, 128.25, 128.77, 129.08, 129.42, 130.08, 130.22, 132.04, 132.57, 133.16, 133.90, 135.77, 148.29, 158.03, 193.91. HRMS (*m/z*) $[M+H]^+$: For $C_{21}H_{16}N_2O_3$ calculated: 345.1234, found: 345.1258.

2-{2-[(1,1′-Biphenyl)-4-yl]-2-oxoethyl}-3-methyl-2,3-dihydrophthalazine-1,4-dione (**5l**): Solid white crystals, yield: 86%, m.p. 194–195°C. ^{1}H NMR (300 MHz, DMSO-d_6, ppm) δ: 3.48 (s, 3H, N–$\underline{CH_3}$), 5.83 (s, 2H, N–$\underline{CH_2}$), 7.42–7.55 (m, 3H, Ar-H), 7.77 (d, J = 7.08 Hz, 2H, Ar-H), 7.89 (d, J = 8.42 Hz, 2H, Ar-H), 7.93–8.02 (m, 2H, Ar-H), 8.10 (t, J = 8.50 Hz, 3H, Ar-H), 8.27 (d, J = 7.32 Hz, 1H, Ar-H). ^{13}C NMR (75 MHz, DMSO-d_6, ppm) δ: 38.88 (N–$\underline{CH_3}$), 69.01 (N–$\underline{CH_2}$), 123.85, 124.20, 126.94, 127.52, 127.58, 128.77, 128.98, 129.60, 133.16, 133.54, 133.91, 139.24, 145.66, 148.25, 158.04, 193.51. HRMS (m/z) $[M+H]^+$: For $C_{23}H_{18}N_2O_3$ calculated: 371.1390, found: 371.1405.

2-Methyl-3-{2-[4-(methylsulfonyl)phenyl]-2-oxoethyl}-2,3-dihydrophthalazine-1,4-dione (**5m**): Solid white crystals, yield: 80%, m.p. 229–230°C. ^{1}H NMR (300 MHz, DMSO-d_6, ppm) δ: 3.32 (s, 3H, S–$\underline{CH_3}$), 3.47 (s, 3H, N–$\underline{CH_3}$), 5.84 (s, 2H, N–$\underline{CH_2}$), 7.92–8.02 (m, 2H, Ar-H), 8.09 (d, J = 7.27 Hz, 1H, Ar-H), 8.13 (d, J = 8.54 Hz, 2H, Ar-H), 8.26 (d, J = 8.48 Hz, 3H, Ar-H). ^{13}C NMR (75 MHz, DMSO-d_6, ppm) δ:

38.85 (N–$\underline{CH_3}$), 43.58 (S–$\underline{CH_3}$), 69.26 (N–$\underline{CH_2}$), 123.81, 124.08, 126.98, 128.04, 128.77, 129.23, 133.25, 133.97, 138.55, 145.27, 148.08, 158.04, 193.89. HRMS (*m/z*) $[M+H]^+$: For $C_{18}H_{16}N_2O_5S$ calculated: 373.0853, found: 373.0852.

4.1.5 | Synthesis of ethyl 2-(3-methyl-1,4-dioxo-3,4-dihydrophthalazin-2(1H)-yl)acetate (6)

Ethyl 2-bromoacetate (10.22 mmol, 1.71 g) was added slowly to a solution of 2-methyl-2,3-dihydrophthalazine-1,4-dione (**4**) (8.51 mmol, 1.5 g) with potassium carbonate K_2CO_3 (15.33 mmol, 2.12 g) in DMF (10 mL). The mixture was stirred for 2 h at room temperature. TLC and CMS were used to keep monitor the reaction. After the reaction was completed, the mixture was poured into iced water and the product was precipitated as a white solid. The resulting product was filtered, washed with water, and dried (83%).

4.1.6 | Synthesis of 2-(3-methyl-1,4-dioxo-3,4-dihydrophthalazin-2(1H)-yl)acetohydrazide (7)

Ethyl 2-(3-methyl-1,4-dioxo-3,4-dihydrophthalazin-2(1*H*)-yl)acetate (**6**) (7.63 mmol, 2 g) and hydrazine hydrate (30.50 mmol of 85% 1.48 mL) were stirred at room temperature overnight in ethanol (75 mL). TLC and CMS were used to monitor the reaction. After the reaction was completed, the mixture was stopped stirring and waited for two phases of solvent and precipitate to form. The precipitated material was filtered. After drying, it was recrystallized from ethanol (88%).

4.1.7 | General procedure for the synthesis of N′-benzylidene-2-(3-methyl-1,4-dioxo-3,4-dihydrophthalazin-2(1H)-yl)acetohydrazide derivatives (8a–8s)

2-(3-Methyl-1,4-dioxo-3,4-dihydrophthalazin-2(1*H*)-yl)acetohydrazide (**7**) (1.01 mmol, 0.25 g) was dissolved in ethanol, and this mixture was added slowly to a solution of Aldehyde derivatives in ethanol (20 mL). The mixture was stirred for 3–5 h at 80°C. TLC and CMS were used to monitor the reaction. After the reaction was completed, the mixture was cold at room temperature, and the product was precipitated. The resulting product was filtered and dried.

N′-Benzylidene-2-(3-methyl-1,4-dioxo-3,4-dihydrophthalazin-2(1*H*)-yl)acetohydrazide (**8a**): Solid white crystals, yield: 91%, m.p. 257–258°C. ^{1}H NMR (300 MHz, DMSO-d_6, ppm) δ: 3.55 (s, 3H, N–$\underline{CH_3}$), 4.93 and 5.42 (s, 2H, N–$\underline{CH_2}$), 7.45 (t, J = 4.71 Hz, 3H, Ar-H), 7.71 (d, J = 7.53 Hz, 2H, Ar-H), 7.91–8.01 (m, 2H, Ar-H), 8.03–8.13 (m, 2H, Ar-H), 8.25 and 8.28 (s, 1H, N=$\underline{CH}$), 11.67, (brs, 1H, N–N–H). ^{13}C NMR (75 MHz, DMSO-d_6, ppm) δ: 63.79 (N–$\underline{CH_3}$), 64.89 (N–$\underline{CH_2}$), 123.90, 126.86, 127.35, 128.74, 129.31, 130.49, 133.08, 133.81, 134.34, 144.39, 144.43, 148.01, 148.62, 158.07, 164.14, 168.70. HRMS (*m/z*) $[M+H]^+$: For $C_{18}H_{16}N_4O_3$ calculated: 337.1295, found: 337.1306.

N′-(4-Bromobenzylidene)-2-(3-methyl-1,4-dioxo-3,4-dihydrophthalazin-2(1*H*)-yl)acetohydrazide (**8b**): Solid white crystals, yield: 83%, m.p. 292–293°C. ^{1}H NMR (300 MHz, DMSO-d_6, ppm) δ: 3.55 (s, 3H, N–$\underline{CH_3}$), 4.93 and 5.42 (s, 2H, N–$\underline{CH_2}$), 7.66 (d, J = 5.33 Hz, 4H, Ar-H), 7.92 (d, J = 7.25 Hz, 1H, Ar-H), 7.97 (d, J = 7.05 Hz, 1H, Ar-H), 7.99–8.02 (m, 1H, Ar-H), 8.05–8.13 (m, 1H, Ar-H), 8.26 and 8.28 (s, 1H, N=$\underline{CH}$), 11.74 (brs, 1H, N–N–H). ^{13}C NMR (75 MHz, DMSO-d_6, ppm) δ: 63.78 (N–$\underline{CH_3}$), 64.87 (N–$\underline{CH_2}$), 123.68, 123.90, 124.34, 126.87, 128.74, 129.24, 129.45, 132.30, 133.10, 133.64, 133.84, 143.27, 148.59, 158.06, 164.25, 168.78. HRMS (*m/z*) $[M+H]^+$: For $C_{18}H_{15}BrN_4O_3$ calculated: 415.0400, found: 415.0412.

N′-(4-Fluorobenzylidene)-2-(3-methyl-1,4-dioxo-3,4-dihydrophthalazin-2(1*H*)-yl)acetohydrazide (**8c**): Solid white crystals, yield: 71%, m.p. 265–266°C. ^{1}H NMR (300 MHz, DMSO-d_6, ppm) δ: 3.56 (s, 3H, N–$\underline{CH_3}$), 4.93 and 5.42 (s, 2H, N–$\underline{CH_2}$), 7.29 (t, J = 9.21 Hz, 2H, Ar-H), 7.78 (d, J = 7.75 Hz, 2H, Ar-H), 7.90–7.98 (m, 2H, Ar-H), 8.00–8.03 (m, 1H, Ar-H), 8.05–8.13 (m, 1H, Ar-H), 8.26 and 8.28 (s, 1H, N=$\underline{CH}$), 11.67 (brs, 1H, N–N–H). ^{13}C NMR (75 MHz, DMSO-d_6, ppm) δ: 63.79 (N–$\underline{CH_3}$), 64.87 (N–$\underline{CH_2}$), 116.22, 123.90, 126.86, 128.74, 129.59, 133.07, 143.26, 146.88, 148.60, 158.06, 161.85, 164.14, 165.13, 168.70. HRMS (*m/z*) $[M+H]^+$: For $C_{18}H_{15}FN_4O_3$ calculated: 355.1201, found: 355.1217.

N′-(4-Chlorobenzylidene)-2-(3-methyl-1,4-dioxo-3,4-dihydrophthalazin-2(1*H*)-yl)acetohydrazide (**8d**): Solid white crystals, yield: 75%, m.p. 282–283°C. ^{1}H NMR (300 MHz, DMSO-d_6, ppm) δ: 3.55 (s, 3H, N–$\underline{CH_3}$), 4.94 and 5.42 (s, 2H, N–$\underline{CH_2}$), 7.51 (d, J = 8.47 Hz, 2H, Ar-H), 7.74 (d, J = 8.55 Hz, 2H, Ar-H), 7.91–7.98 (m, 2H, Ar-H), 7.99–8.02 (m, 1H, Ar-H), 8.05–8.13 (m, 1H, Ar-H), 8.26 and 8.28 (s, 1H, N=$\underline{CH}$), 11.73 (brs, 1H, N–N–H). ^{13}C NMR (75 MHz, DMSO-d_6, ppm) δ: 63.78 (N–$\underline{CH_3}$), 64.87 (N–$\underline{CH_2}$), 123.90, 124.34, 126.86, 128.74, 129.00, 129.39, 133.09, 133.30, 133.81, 134.88, 143.13, 146.67, 148.59, 158.07, 164.23, 168.77. HRMS (*m/z*) $[M+H]^+$: For $C_{18}H_{15}ClN_4O_3$ calculated: 371.0905, found: 371.0919.

2-(3-Methyl-1,4-dioxo-3,4-dihydrophthalazin-2(1*H*)-yl)-*N′*-(4-methylbenzylidene)acetohydrazide (**8e**): Solid white crystals, yield: 84%, m.p. 260–261°C. ^{1}H NMR (300 MHz, DMSO-d_6, ppm) δ: 2.34 (s, 3H, Ph–$\underline{CH_3}$), 3.55 (s, 3H, N–$\underline{CH_3}$), 4.92 and 5.41 (s, 2H, N–$\underline{CH_2}$), 7.26 (d, J = 8.01 Hz, 2H, Ar-H), 7.60 (d, J = 8.07 Hz, 2H, Ar-H), 7.90–7.96 (m, 2H, Ar-H), 7.97–8.02 (m, 1H, Ar-H), 8.05–8.13 (m, 1H, Ar-H), 8.25 and 8.28 (s, 1H, N=$\underline{CH}$), 11.60 (brs, 1H, N–N–H). ^{13}C NMR (75 MHz, DMSO-d_6, ppm) δ: 21.48 (Ph–$\underline{CH_3}$), 63.79 (N–$\underline{CH_3}$), 64.89 (N–$\underline{CH_2}$), 123.91, 124.36, 126.86, 127.32, 128.74, 129.90, 131.64, 133.07, 133.80, 140.27, 144.47, 144.51, 148.62, 158.06, 164.00, 168.57. HRMS (*m/z*) $[M+H]^+$: For $C_{19}H_{18}N_4O_3$ calculated: 351.1452, found: 351.1468.

N′-(4-Methoxybenzylidene)-2-(3-methyl-1,4-dioxo-3,4-dihydrophthalazin-2(1*H*)-yl)acetohydrazide (**8f**): Solid white crystals, yield: 86%, m.p. 263–264°C. ^{1}H NMR (300 MHz, DMSO-d_6, ppm) δ: 3.56 (s, 3H, N–$\underline{CH_3}$), 3.80 (s, 3H, Ph–O$\underline{CH_3}$), 4.91 and 5.40 (s, 2H, N–CH_2), 7.01 (d, J = 8.78 Hz, 2H, Ar-H), 7.65 (d, J = 8.75 Hz, 2H, Ar-H), 7.90–8.01 (m, 3H, Ar-H), 8.05–8.13 (m, 1H, Ar-H), 8.24 and

8.28 (s, 1H, N=CH), 11.54 (brs, 1H, N–N–H). ^{13}C NMR (75 MHz, DMSO-d_6, ppm) δ: 55.77 (Ph–OCH_3), 63.79 (N–CH_3), 64.89 (N–CH_2), 114.77, 123.91, 124.37, 126.85, 126.92, 128.74, 128.94, 129.20, 133.06, 133.80, 144.25, 148.63, 158.06, 161.18, 163.84, 168.43. APCI (m/z) $[M+H]^+$: For $C_{19}H_{18}N_4O_4$ calculated: 367.14, found: 367.1.

N′-(3,5-Dimethoxybenzylidene)-2-(3-methyl-1,4-dioxo-3,4-dihydrophthalazin-2(1*H*)-yl)acetohydrazide (**8g**): Solid white crystals, yield: 79%, m.p. 244–245°C. ^{1}H NMR (300 MHz, DMSO-d_6, ppm) δ: 3.56 (s, 3H, N–CH_3), 3.78 (s, 6H, Ph–OCH_3), 4.93 and 5.42 (s, 2H, N–CH_2), 6.56 (d, *J* = 4.45 Hz, 1H, Ar-H), 6.87 (t, *J* = 4.56 Hz, 2H, Ar-H), 7.91–8.01 (m, 3H, Ar-H), 8.05–8.13 (m, 1H, Ar-H), 8.20 and 8.27 (s, 1H, N=CH), 11.72 (brs, 1H, N–N–H). ^{13}C NMR (75 MHz, DMSO-d_6, ppm) δ: 55.78 (Ph–OCH_3), 63.85 (N–CH_3), 64.86 (N–CH_2), 102.52, 105.11, 105.26, 123.89, 124.33, 126.87, 128.72, 133.10, 133.84, 136.33, 144.11, 148.60, 158.06, 161.11, 164.20, 168.77. HRMS (*m/z*) $[M+H]^+$: For $C_{20}H_{20}N_4O_5$ calculated: 397.1506, found: 397.1522.

N′-(3,4-Dihydroxybenzylidene)-2-(3-methyl-1,4-dioxo-3,4-dihydrophthalazin-2(1*H*)-yl)acetohydrazide (**8h**): Solid white crystals, yield: 89%, m.p. 296–297°C. ^{1}H NMR (300 MHz, DMSO-d_6, ppm) δ: 3.56 (s, 3H, N–CH_3), 4.90 and 5.38 (s, 2H, N–CH_2), 6.79 (d, *J* = 8.15 Hz, 1H, Ar-H), 6.94 (d, *J* = 8.20 Hz, 1H, Ar-H), 7.20 (d, *J* = 11.15 Hz, 1H, Ar-H), 7.85 (s, 1H, Ar-H), 7.91–8.01 (m, 2H, Ar-H), 8.05–8.13 (m, 1H, Ar-H), 8.25 and 8.28 (s, 1H, N=CH), 11.44 (brs, 1H, N–N–H). ^{13}C NMR (75 MHz, DMSO-d_6, ppm) δ: 63.71 (N–CH_3), 64.87 (N–CH_2), 113.06, 116.04, 120.68, 123.93, 124.37, 125.75, 126.85, 128.73, 133.08, 133.80, 145.01, 146.12, 148.32, 158.06, 163.67, 168.22. HRMS (*m/z*) $[M+H]^+$: For $C_{18}H_{16}N_4O_5$ calculated: 369.1193, found: 369.1183.

2-(3-Methyl-1,4-dioxo-3,4-dihydrophthalazin-2(1*H*)-yl)-*N′*-(naphthalen-1-ylmethylene)acetohydrazide (**8i**): Solid white crystals, yield: 86%, m.p. 232–233°C. ^{1}H NMR (300 MHz, DMSO-d_6, ppm) δ: 3.56 (s, 3H, N–CH_3), 4.99 and 5.50 (s, 2H, N–CH_2), 7.60 (t, *J* = 7.29 Hz, 2H, Ar-H), 7.68 (d, *J* = 8.46 Hz, 1H, Ar-H), 7.92 (d, *J* = 7.24 Hz, 2H, Ar-H), 7.96–8.04 (m, 3H, Ar-H), 8.07–8.17 (m, 1H, Ar-H), 8.26 and 8.28 (s, 1H, N=CH), 11.74 (brs, 1H, N-N-H). ^{13}C NMR (75 MHz, DMSO-d_6, ppm) δ: 63.93 (N–CH_3), 64.98 (N–CH_2), 123.90, 124.25, 126.03, 126.80, 127.93, 128.09, 128.76, 129.35, 129.56, 130.45, 131.00, 133.10, 133.85, 133.98, 144.32, 148.08, 148.63, 158.07, 164.18, 168.65. HRMS (*m/z*) $[M+H]^+$: For $C_{22}H_{18}N_4O_3$ calculated: 387.1452, found: 387.1467.

2-(3-Methyl-1,4-dioxo-3,4-dihydrophthalazin-2(1*H*)-yl)-*N′*-(naphthalen-2-ylmethylene)acetohydrazide (**8j**): Solid white crystals, yield: 81%, m.p. 244–245°C. ^{1}H NMR (300 MHz, DMSO-d_6, ppm) δ: 3.57 (s, 3H, N–CH_3), 4.97 and 5.49 (s, 2H, N–CH_2), 7.55–7.60 (m, 2H, Ar-H), 7.91–8.02 (m, 6H, Ar-H), 8.07–8.16 (m, 2H, Ar-H), 8.19 (s, 1H, Ar-H), 8.27 and 8.44 (s, 1H, N=CH), 11.80 (brs, 1H, N–N–H). ^{13}C NMR (75 MHz, DMSO-d_6, ppm) δ: 63.86 (N–CH_3), 64.89 (N–CH_2), 122.77, 123.92, 124.35, 126.87, 127.27, 127.60, 128.26, 128.78, 128.98, 129.27, 132.04, 133.28, 133.83, 134.12, 144.48, 147.90, 148.62, 158.07, 164.18, 168.74. HRMS (m/z) $[M+H]^+$: For $C_{22}H_{18}N_4O_3$ calculated: 387.1452, found: 387.1471.

N′-[(6-Methoxynaphthalen-2-yl)methylene]-2-(3-methyl-1,4-dioxo-3,4-dihydrophthalazin-2(1*H*)-yl)acetohydrazide (**8k**): Solid white crystals, yield: 77%, m.p. 231–232°C. ^{1}H NMR (300 MHz, DMSO-d_6, ppm) δ: 3.57 (s, 3H, N–CH_3), 3.90 (s, 3H, Naphth-OCH_3), 4.95 and 5.47 (s, 2H, N–CH_2), 7.21 (dd, J_1 = 2.51 Hz, J_2 = 8.89 Hz 1H, Ar-H), 7.37 (s, 1H, Ar-H), 7.88 (t, *J* = 4.07 Hz, 2H, Ar-H), 7.91–7.99 (m, 3H, Ar-H), 8.04–8.12 (m, 2H, Ar-H), 8.14 (s, 1H, Ar-H), 8.27 and 8.39 (s, 1H, N=CH), 11.71 (brs, 1H, N–N–H). ^{13}C NMR (75 MHz, DMSO-d_6, ppm) δ: 55.78 (Naphth-OCH_3), 63.86 (N–CH_3), 64.90 (N–CH_2), 106.75, 119.65, 123.34, 123.93, 124.36, 126.87, 127.89, 128.57, 129.09, 129.78, 130.37, 133.11, 133.83, 135.69, 144.71, 148.63, 158.07, 158.67, 164.02, 168.61. HRMS (m/z) $[M+H]^+$: For $C_{23}H_{20}N_4O_4$ calculated: 417.1557, found: 417.1585.

2-(3-Methyl-1,4-dioxo-3,4-dihydrophthalazin-2(1*H*)-yl)-*N′*-(thiophen-2-ylmethylene)acetohydrazide (**8l**): Solid white crystals, yield: 76%, m.p. 236–237°C. ^{1}H NMR (300 MHz, DMSO-d_6, ppm) δ: 3.56 (s, 3H, N–CH_3), 4.91 and 5.33 (s, 2H, N–CH_2), 7.14 (t, *J* = 5.11 Hz, 1H, Ar-H), 7.47 (t, *J* = 4.02 Hz, 1H, Ar-H), 7.67 (t, *J* = 5.40 Hz, 1H, Ar-H), 7.91–8.02 (m, 2H, Ar-H), 8.04–8.13 (m, 1H, Ar-H), 8.21 and 8.51 (s, 1H, N=CH), 8.27 (d, *J* = 7.16 Hz, 1H, Ar-H), 11.64 (brs, 1H, N–N–H). ^{13}C NMR (75 MHz, DMSO-d_6, ppm) δ: 63.56 (N–CH_3), 64.89 (N–CH_2), 123.90, 126.87, 128.44, 129.11, 131.22, 131.70, 133.10, 133.83, 139.56, 143.22, 148.58, 158.07, 163.95, 168.31. HRMS (*m/z*) $[M+H]^+$: For $C_{16}H_{14}N_4O_3S$ calculated: 343.0859, found: 343.0869.

N′-(Furan-2-ylmethylene)-2-(3-methyl-1,4-dioxo-3,4-dihydrophthalazin-2(1*H*)-yl)acetohydrazide (**8m**): Solid white crystals, yield: 82%, m.p. 237–238°C. ^{1}H NMR (300 MHz, DMSO-d_6, ppm) δ: 3.55 (s, 3H, N–CH_3), 4.90 and 5.33 (s, 2H, N–CH_2), 6.62–6.64 (m, 1H, Ar-H), 6.92 (d, *J* = 3.39 Hz, 1H, Ar-H), 7.84–7.90 (m, 2H, Ar-H), 7.92–8.00 (m, 2H, Ar-H), 8.04–8.12 (m, 1H, Ar-H), 8.04–8.13 (m, 1H, Ar-H), 8.17 and 8.25 (s, 1H, N=CH), 11.62 (brs, 1H, N–N–H). ^{13}C NMR (75 MHz, DMSO-d_6, ppm) δ: 63.65 (N–CH_3), 64.88 (N–CH_2), 112.65, 114.47, 123.90, 126.87, 128.74, 133.10, 133.82, 134.48, 145.59, 148.58, 149.30, 158.05, 164.05, 168.48. HRMS (*m/z*) $[M+H]^+$: For $C_{16}H_{14}N_4O_4$ calculated: 327.1088, found: 327.1087.

N′-[(1*H*-Pyrrol-2-yl)methylene]-2-(3-methyl-1,4-dioxo-3,4-dihydrophthalazin-2(1*H*)-yl)acetohydrazide (**8n**): Solid white crystals, yield: 87%, m.p. 254–255°C. ^{1}H NMR (300 MHz, DMSO-d_6, ppm) δ: 3.56 (s, 3H, N–CH_3), 4.88 and 5.38 (s, 2H, N–CH_2), 6.11–6.14 (m, 1H, Ar-H), 6.44–6.48 (m, 1H, Ar-H), 6.89–6.96 (m, 1H, Ar-H), 7.84 (s, 1H, –NH), 7.90–8.00 (m, 2H, Ar-H), 8.05–8.09 (m, 1H, Ar-H), 8.12 and 8.25 (s, 1H, N=CH), 11.33 (brs, 1H, N–N–H). ^{13}C NMR (75 MHz, DMSO-d_6, ppm) δ: 64.01 (N–CH_3), 64.96 (N–CH_2), 109.71, 113.12, 122.50, 123.97, 126.85, 128.76, 133.07, 133.80, 137.06, 141.19, 148.71, 158.08, 163.34, 168.14. HRMS (m/z) $[M+H]^+$: For $C_{16}H_{15}N_5O_3$ calculated: 326.1248, found: 326.1264.

N′-(5-Bromo-2-hydroxybenzylidene)-2-(3-methyl-1,4-dioxo-3,4-dihydrophthalazin-2(1*H*)-yl)acetohydrazide (**8o**): Solid white crystals, yield: 77%, m.p. 264–265°C. ^{1}H NMR (300 MHz, DMSO-d_6, ppm) δ: 3.55 (s, 3H, N–CH_3), 4.94 and 5.41 (s, 2H, N–CH_2), 6.88 (dd, J_1 = 3.39 Hz, J_2 = 8.86 Hz, 1H, Ar-H), 7.41 (t, *J* = 8.88 Hz, 1H, Ar-H), 7.75–7.83 (m, 1H, Ar-H), 7.90–8.01 (m, 2H, Ar-H), 8.04–8.13 (m, 1H, Ar-H), 8.25 and 8.47 (s, 2H, N=CH and Ar-H), 11.67 (brs, 1H, N–N–H). ^{13}C NMR (75 MHz, DMSO-d_6, ppm) δ: 63.89 (N–CH_3), 64.81 (N–CH_2), 111.30, 118.87, 121.76, 122.91, 123.90, 126.87,

128.74, 130.46, 133.82, 139.54, 145.46, 148.59, 156.02, 158.06, 164.26, 168.65. HRMS (*m/z*) $[M+H]^+$: For $C_{18}H_{15}BrN_4O_4$ calculated: 431.0349, found: 431.0357.

2-(3-Methyl-1,4-dioxo-3,4-dihydrophthalazin-2(1*H*)-yl)-*N*′-(2-nitrobenzylidene)acetohydrazide (**8p**): Solid white crystals, yield: 80%, m.p 267–268°C. ^{1}H NMR (300 MHz, DMSO-d_6, ppm) δ: 3.55 (s, 3H, N–$\underline{CH_3}$), 4.97 and 5.42 (s, 2H, N–$\underline{CH_2}$), 7.65–7.71 (m, 1H, Ar-H), 7.81 (t, *J* = 7.53 Hz, 1H, Ar-H), 7.91–8.01 (m, 2H, Ar-H), 8.08 (t, *J* = 7.84 Hz, 3H, Ar-H), 8.27 (d, *J* = 7.17 Hz, 1H, Ar-H), 8.40 and 8.69 (s, 1H, N=$\underline{CH}$), 11.96 (brs, 1H, N–N–H). ^{13}C NMR (75 MHz, DMSO-d_6, ppm) δ: 63.73 (N–$\underline{CH_3}$), 64.83 (N–$\underline{CH_2}$), 123.88, 125.06, 126.87, 128.49, 128.73, 128.83, 131.08, 133.10, 133.83, 134.03, 140.00, 143.45, 148.46, 158.06, 164.58, 169.01. HRMS (m/z) $[M+H]^+$: For $C_{18}H_{15}N_5O_5$ calculated: 382.1146, found: 382.1160.

2-(3-Methyl-1,4-dioxo-3,4-dihydrophthalazin-2(1*H*)-yl)-*N*′-(3-nitrobenzylidene)acetohydrazide (**8q**): Solid white crystals, yield: 87%, m.p. 275–276°C. ^{1}H NMR (300 MHz, DMSO-d_6, ppm) δ: 3.56 (s, 3H, N–$\underline{CH_3}$), 4.97 and 5.46 (s, 2H, N–$\underline{CH_2}$), 7.73 (t, *J* = 7.96 Hz, 1H, Ar-H), 7.90–8.00 (m, 2H, Ar-H), 8.04–8.10 (m, 1H, Ar-H), 8.12–8.18 (m, 2H, Ar-H), 8.23–8.27 (m, 2H, Ar-H), 8.41 and 8.50 (s, 1H, N=$\underline{CH}$), 11.93 (brs, 1H, N–N–H). ^{13}C NMR (75 MHz, DMSO-d_6, ppm) δ: 63.80 (N–$\underline{CH_3}$), 64.82 (N–$\underline{CH_2}$), 121.49, 123.85, 124.29, 124.66, 126.85, 128.72, 130.88, 133.42, 133.79, 136.18, 142.14, 145.56, 148.63, 158.04, 164.54, 168.98. HRMS (*m/z*) $[M+H]^+$: For $C_{18}H_{15}N_5O_5$ calculated: 382.1146, found: 382.1158.

N′-(2,6-Dichlorobenzylidene)-2-(3-methyl-1,4-dioxo-3,4-dihydrophthalazin-2(1*H*)-yl)acetohydrazide (**8r**): Solid white crystals, yield: 74%, m.p. 271–272°C. ^{1}H NMR (300 MHz, DMSO-d_6, ppm) δ: 3.54 (s, 3H, N–$\underline{CH_3}$), 4.96 and 5.35 (s, 2H, N–$\underline{CH_2}$), 7.44 (t, *J* = 7.33 Hz, 1H, Ar-H), 7.58 (d, *J* = 7.74 Hz, 2H, Ar-H), 7.89–8.00 (m, 2H, Ar-H), 8.03–8.12 (m, 1H, Ar-H), 8.04–8.13 (m, 1H, Ar-H), 8.23–8.27 and 8.48 (m, 2H, N=$\underline{CH}$ and Ar-H), 11.92 (brs, 1H, N–N–H). ^{13}C NMR (75 MHz, DMSO-d_6, ppm) δ: 63.78 (N–$\underline{CH_3}$), 64.87 (N–$\underline{CH_2}$), 123.85, 124.30, 126.88, 128.76, 129.51, 129.92, 131.62, 133.09, 133.82, 134.40, 139.33, 148.54, 158.06, 169.09. HRMS (*m/z*) $[M+H]^+$: For $C_{18}H_{14}Cl_2N_4O_3$ calculated: 405.0516, found: 405.0518.

N′-(3,4-Dichlorobenzylidene)-2-(3-methyl-1,4-dioxo-3,4-dihydrophthalazin-2(1*H*)-yl)acetohydrazide (**8s**): Solid white crystals, yield: 71%, m.p. 267–268°C. ^{1}H NMR (300 MHz, DMSO-d_6, ppm) δ: 3.56 (s, 3H, N–$\underline{CH_3}$), 4.94 and 5.43 (s, 2H, N–$\underline{CH_2}$), 7.69 (s, 2H, N=$\underline{CH}$ and Ar-H), 7.90–7.97 (m, 3H, Ar-H), 8.01–8.07 (m, 2H, Ar-H), 8.27 (d, *J* = 7.26 Hz, 1H, Ar-H), 11.73 (brs, 1H, N–N–H). ^{13}C NMR (75 MHz, DMSO-d_6, ppm) δ: 63.91 (N–$\underline{CH_3}$), 64.96 (N–$\underline{CH_2}$), 120.22, 123.87, 124.11, 126.87, 127.26, 128.83, 131.50, 133.03, 133.73, 135.27, 141.83, 168.91. HRMS (*m/z*) $[M+H]^+$: For $C_{18}H_{14}Cl_2N_4O_3$ calculated: 405.0516, found: 405.0535.

4.2 | Prediction of physicochemical and pharmacokinetic properties

Drug discovery and development is an expensive and time-consuming process. Drug candidates should exhibit high biological activity with low toxicity. Due to this crucial qualification, achieving therapeutic concentration and targeting the organism are equally important. The traditional approach to evaluating pharmacokinetics involves breaking down the various effects associated with reaching the target into different parameters. The ADME characteristics of compounds were calculated using previously published methodologies.[26,35,37–39]

4.3 | Investigation of anti-AChE and anti-BChE activity

The AChE and BChE inhibitory potencies of the produced compounds (**5a–5m and 8a–8s**) were determined in vitro using a modified Ellman's spectrophotometric technique.[40] Sigma-Aldrich and Fluka provided the reagents and materials utilized in the enzyme inhibition experiment. The cholinesterase enzyme inhibition technique described in earlier research articles was used.[41,42] As enzymes, human AChE (CAS no.: 9000-81-1) and human butyrylcholinesterase (CAS no.: 9001-08-5) were employed.

4.4 | Enzyme kinetics studies of the ChE enzyme

The experimental protocols for the kinetic studies were exactly the same as those for the inhibition studies. However, unlike the inhibition method, the compounds were used at the calculated concentrations of 2 × IC_{50}, IC_{50}, and IC_{50}/2. For the ChE enzymes, the substrate (acetylthiocholine iodide (ATC) solution) was used with serial dilutions at 6 different concentrations (600, 300, 150, 75, 37.5, and 18.75 μM). The measurements were carried out separately with and without an inhibitor. The obtained absorbance values were analyzed against varying substrate concentrations in the Microsoft Office Excel-2013 software, and Lineweaver–Burk plots were drawn.[41,43–45]

4.5 | In vitro BBB permeability assay

To observe the BBB crossing ability of the most active compounds (**8m**, **8n,** and **8p**), the PAMPA was performed as previously described.[46,47]

4.6 | In silico studies

4.6.1 | Molecular docking studies

The structure-based in silico docking approach was used to assess the potential binding and interaction points of the most active compounds (**8m**, **8n**, and **8o**) that were demonstrated to be effective at the AChE enzyme active sites. Molecular docking was conducted with the assistance of Schrödinger's Maestro Interface 2020. Protein–ligand interaction studies were performed using the crystal structure of AChE

(PDB code 4EY7),[48] which was obtained from the Protein Data Bank (PDB) and processed using Schrödinger's Maestro Protein Preparation Wizard program. The molecular docking of active compounds was conducted using previously published methodologies.[49,50]

4.6.2 | Molecular dynamic simulation (MDS) studies

Molecular dynamic (MD) simulations are widely recognized as a necessary computational approach for determining a ligand's time-dependent stability in an active site of a drug–receptor combination.[31] To ensure the stability of the docking result's discovered hits, MD simulations lasting 100 ns were performed. The molecular dynamics of active compounds were studied using previously published methodologies.[32,35,37,38]

4.6.3 | DFT studies

The Gaussian 09 W package[33] and GaussView 5.0[34] molecular visualization programs were used to perform theoretical approaches for the targeted compounds (**5a–5m** and **8a–8s**). DFT studies of targeted compounds were studied using previously published methodologies.[26,37,38,51]

ACKNOWLEDGMENTS

The authors present their thanks to MERLAB (formerly DOPNA) laboratory, Anadolu University, and Scientific Research Projects, Anadolu University. The authors have no funding to report.

CONFLICTS OF INTEREST STATEMENT

The authors declare no conflicts of interest.

DATA AVAILABILITY STATEMENT

Data that support the findings of this study are available from the corresponding author upon reasonable request.

ORCID

Demokrat Nuha http://orcid.org/0000-0002-7271-6791
Asaf Evrim Evren http://orcid.org/0000-0002-8651-826X

REFERENCES

[1] A. Slachevsky, G. Forno, P. Barraza, E. Mioshi, C. Delgado, P. Lillo, F. Henriquez, E. Bravo, M. Farias, C. Muñoz-Neira, A. Ibañez, M. A. Parra, M. Hornberger, *J. Neurol.* **2019**, *266*(6), 1310. https://doi.org/10.1007/s00415-019-09260-w

[2] C. Brodeur, É. Belley, L. M. Deschênes, A. Enriquez-Rosas, M. Hubert, A. Guimond, J. Bilodeau, J. P. Soucy, J. Macoir, *Life* **2022**, *12*(5), 662. https://doi.org/10.3390/life12050662

[3] A. L. Turcu, J. Companys-Alemany, M. B. Phillips, D. S. Patel, C. Griñán-Ferré, M. I. Loza, J. M. Brea, B. Pérez, D. Soto, F. X. Sureda, M. G. Kurnikova, J. W. Johnson, M. Pallàs, S. Vázquez, *Eur. J. Med. Chem.* **2022**, *236*, 114354. https://doi.org/10.1016/j.ejmech.2022.114354

[4] L. Cong, X. Dong, Y. Wang, Y. Deng, B. Li, R. Dai, *Eur. J. Med. Chem.* **2019**, *166*, 11. https://doi.org/10.1016/j.ejmech.2019.01.039

[5] M. Wu, J. Ma, L. Ji, M. Wang, J. Han, Z. Li, *Eur. J. Med. Chem.* **2019**, *177*, 198. https://doi.org/10.1016/j.ejmech.2019.05.055

[6] Z. Sang, K. Wang, J. Shi, W. Liu, X. Cheng, G. Zhu, Y. Wang, Y. Zhao, Z. Qiao, A. Wu, Z. Tan, *Eur. J. Med. Chem.* **2020**, *192*, 112180. https://doi.org/10.1016/j.ejmech.2020.112180

[7] J. Nielsen, P. H. Rasmussen, *Tetrahedron Lett.* **1996**, *37*(19), 3351. https://doi.org/10.1016/0040-4039(96)00544-8

[8] M. B. Teimouri, *Tetrahedron* **2006**, *62*(47), 10849. https://doi.org/10.1016/j.tet.2006.09.006

[9] H. Almahli, E. Hadchity, M. Y. Jaballah, R. Daher, H. A. Ghabbour, M. M. Kabil, N. S. Al-Shakliah, W. M. Eldehna, *Bioorg. Chem.* **2018**, *77*, 443. https://doi.org/10.1016/j.bioorg.2018.01.034

[10] S. M. Chang, V. Jain, T. L. Chen, A. S. Patel, H. B. Pidugu, Y. W. Lin, M. H. Wu, J. R. Huang, H. C. Wu, A. Shah, T. L. Su, T. C. Lee, *J. Med. Chem.* **2019**, *62*(5), 2404. https://doi.org/10.1021/acs.jmedchem.8b01689

[11] L. Jalili-Baleh, H. Nadri, A. Moradi, S. N. A. Bukhari, M. Shakibaie, M. Jafari, M. Golshani, F. Homayouni Moghadam, L. Firoozpour, A. Asadipour, S. Emami, M. Khoobi, A. Foroumadi, *Eur. J. Med. Chem.* **2017**, *139*, 280. https://doi.org/10.1016/j.ejmech.2017.07.072

[12] S. Demirayak, A. C. Karaburun, R. Beis, *Eur. J. Med. Chem.* **2004**, *39*(12), 1089. https://doi.org/10.1016/j.ejmech.2004.09.005

[13] R. Sivakumar, S. Kishore Gnanasam, S. Ramachandran, J. Thomas Leonard, *Eur. J. Med. Chem.* **2002**, *37*, 793.

[14] W. Pakulska, Z. Malinowski, A. K. Szczesniak, E. Czarnecka, J. Epsztajn, *Arch. Pharm.* **2009**, *342*(1), 41. https://doi.org/10.1002/ardp.200800016

[15] A. M. Sridhara, K. R. Venugopala Reddy, J. Keshavayya, P. S. Kumar Goud, B. C. Somashekar, P. Bose, S. K. Peethambar, S. K. Gaddam, *Eur. J. Med. Chem.* **2010**, *45*(11), 4983. https://doi.org/10.1016/j.ejmech.2010.08.005

[16] M. S. M. Abd Alla, M. I. Hegab, N. A. Abo Taleb, S. M. Hasabelnaby, A. Goudah, *Eur. J. Med. Chem.* **2010**, *45*(4), 1267. https://doi.org/10.1016/j.ejmech.2009.10.028

[17] M. Van der Mey, H. Boss, D. Couwenberg, A. Hatzelmann, G. J. Sterk, K. Goubitz, H. Schenk, H. Timmerman, *J. Med. Chem.* **2002**, *45*(12), 2526.

[18] F. M. Awadallah, W. I. el-Eraky, D. O. Saleh, *Eur. J. Med. Chem.* **2012**, *52*, 14. https://doi.org/10.1016/j.ejmech.2012.02.051

[19] M. H. Norman, G. C. Rigdon, F. Navas, B. R. Cooper, *J. Med. Chem.* **1994**, *37*, 2552.

[20] D. Simijonović, E. E. N. Vlachou, K. E. Litinas, Z. D. Petrović, V. P. Petrović, *J. Mol. Struct.* **2021**, *1226*, 129366. https://doi.org/10.1016/j.molstruc.2020.129366

[21] M. A. V. Ribeiro da Silva, J. I. T. A. Cabral, *J. Chem. Thermodyn.* **2008**, *40*(5), 829. https://doi.org/10.1016/j.jct.2008.01.010

[22] W. Hussein, B. N. Sağlık, S. Levent, B. Korkut, S. Ilgın, Y. Özkay, Z. A. Kaplancıklı, *Molecules* **2018**, *23*(8), 2033. https://doi.org/10.3390/molecules23082033

[23] A. E. Evren, D. Nuha, S. Dawbaa, B. N. Sağlık, L. Yurttaş, *Eur. J. Med. Chem.* **2022**, *229*, 114097. https://doi.org/10.1016/j.ejmech.2021.114097

[24] J. Wang, B. J. Gu, C. L. Masters, Y. J. Wang, *Nat. Rev. Neurol.* **2017**, *13*(10), 612. https://doi.org/10.1038/nrneurol.2017.111

[25] J. Shi, M. N. Sabbagh, B. Vellas, *BMJ* **2020**, *371*, m3684. https://doi.org/10.1136/bmj.m3684

[26] D. Nuha, A. E. Evren, Z. Ş. Çiyanci, H. E. Temel, G. Akalin Çiftçi, L. Yurttaş, *Arch. Pharm.* **2022**, *355*(9), e2200105. https://doi.org/10.1002/ardp.202200105

[27] M. Jatczak, K. Muylaert, L. M. De Coen, J. Keemink, B. Wuyts, P. Augustijns, C. V. Stevens, *Bioorg. Med. Chem.* **2014**, *22*(15), 3947. https://doi.org/10.1016/j.bmc.2014.06.009

[28] A. Daina, O. Michielin, V. Zoete, *Sci. Rep.* **2017**, *7*(1), 42717. https://doi.org/10.1038/srep42717
[29] H. L. Wong, X. Y. Wu, R. Bendayan, *Adv. Drug Delivery Rev.* **2012**, *64*(7), 686. https://doi.org/10.1016/j.addr.2011.10.007
[30] B. N. Sağlik, Doctoral thesis. Anadolu University **2019**.
[31] X. Liu, D. Shi, S. Zhou, H. Liu, H. Liu, X. Yao, *Expert Opin. Drug Discovery* **2018**, *13*(1), 23. https://doi.org/10.1080/17460441.2018.1403419
[32] A. A. Al-Sharabi, S. Saffour, A. E. Evren, G. Bayazıt, G. Çongur, Ü. D. Gül, L. Yurttaş, *J. Mol. Struct.* **2023**, *1289*, 135775. https://doi.org/10.1016/j.molstruc.2023.135775
[33] M. Frisch, G. Trucks, H. Schlegel, G. Scuseria, M. Robb, J. Cheeseman, G. Scalmani, V. Barone, B. Mennucci, G. Petersson. Gaussian09, Revision A, Vol. 121 (in series), Wallingford CT Inc., **2009**.
[34] A. Galano, J. R. Alvarez-Idaboy, *J. Comput. Chem.* **2013**, *34*(28), 2430. https://doi.org/10.1002/jcc.23409
[35] D. Nuha, A. E. Evren, Z. Ş. Çiyanci, H. E. Temel, G. Akalin Çiftci, L. Yurttas, *Cumhuriyet Sci. J.* **2022**, *43*(4), 584. https://doi.org/10.17776/csj.1128672
[36] K. Fukui, *Science* **1982**, *218*(4574), 747.
[37] S. Dawbaa, D. Nuha, A. E. Evren, M. Y. Cankiliç, L. Yurttaş, G. Turan, *J. Mol. Struct.* **2023**, *1282*, 135213.
[38] D. Nuha, A. E. Evren, Ö. Kapusiz, Ü. D. Gül, N. Gundogdu-Karaburun, A. Ç. Karaburun, H. Berber, *J. Mol. Struct.* **2023**, *1272*, 134166. https://doi.org/10.1016/j.molstruc.2022.134166
[39] D. Nuha, A. E. Evren, M. Yılmaz Cankılıç, L. Yurttaş, *Phosphorus, Sulfur Silicon Relat. Elem.* **2021**, *196*(10), 954. https://doi.org/10.1080/10426507.2021.1946537
[40] K. D. C. George, L. Ellman, J. R. Valentino Andres, R. O. B. E. R. T. M. Featherstone, *Biochem. Pharmacol.* **1961**, *7*, 88.
[41] B. N. Sağlık, S. Ilgın, Y. Özkay, *Eur. J. Med. Chem.* **2016**, *124*, 1026. https://doi.org/10.1016/j.ejmech.2016.10.042
[42] Ş. Karaca, D. Osmaniye, B. N. Sağlık, S. Levent, S. Ilgın, Y. Özkay, A. Ç. Karaburun, Z. A. Kaplancıklı, N. Gundogdu-Karaburun, *RSC Adv.* **2022**, *12*(36), 23626. https://doi.org/10.1039/d2ra03803j
[43] F. Tok, B. Koçyiğit-Kaymakçıoğlu, B. N. Sağlık, S. Levent, Y. Özkay, Z. A. Kaplancıklı, *Bioorg. Chem.* **2019**, *84*, 41.
[44] D. Osmaniye, A. E. Evren, B. N. Sağlık, S. Levent, Y. Özkay, Z. A. Kaplancıklı, *Arch. Pharm.* **2022**, *355*(3), e2100450. https://doi.org/10.1002/ardp.202100450
[45] Ö. D. Can, D. Osmaniye, Ü. Demir Özkay, B. N. Sağlık, S. Levent, S. Ilgın, M. Baysal, Y. Özkay, Z. A. Kaplancıklı, *Eur. J. Med. Chem.* **2017**, *131*, 92. https://doi.org/10.1016/j.ejmech.2017.03.009
[46] B. N. Sağlık, D. Osmaniye, U. Acar Çevik, S. Levent, B. Kaya Çavuşoğlu, Y. Özkay, Z. A. Kaplancıklı, *Molecules* **2020**, *25*(18), 4312. https://doi.org/10.3390/molecules25184312
[47] G. Yan, L. Hao, Y. Niu, W. Huang, W. Wang, F. Xu, L. Liang, C. Wang, H. Jin, P. Xu, *Eur. J. Med. Chem.* **2017**, *137*, 462. https://doi.org/10.1016/j.ejmech.2017.06.020
[48] J. Cheung, M. J. Rudolph, F. Burshteyn, M. S. Cassidy, E. N. Gary, J. Love, M. C. Franklin, J. J. Height, *J. Med. Chem.* **2012**, *55*(22), 10282. https://doi.org/10.1021/jm300871x
[49] A. E. Evren, D. Nuha, L. Yurttaş, *Eur. J. Life Sci.* **2023**, *1*(3), 118. https://doi.org/10.55971/ejls.1209591
[50] A. E. Evren, S. Dawbaa, D. Nuha, Ş. A. Yavuz, Ü. D. Gül, L. Yurttaş, *J. Mol. Struct.* **2021**, *1241*, 130692. https://doi.org/10.1016/j.molstruc.2021.130692
[51] H. B. D. emokrat NUHA, *Network* **2022**, *1*, 1.

SUPPORTING INFORMATION

Additional supporting information can be found online in the Supporting Information section at the end of this article.

How to cite this article: D. Nuha, A. E. Evren, B. N. S. Özkan, N. Gundogdu-Karaburun, A. Ç. Karaburun, *Arch. Pharm.* **2024**;*357*:e2400067. https://doi.org/10.1002/ardp.202400067